EUROPEAN JOURNAL OF PURE AND APPLIED MATHEMATICS
Vol. 17, No. 4, 2024, 2763-2799
ISSN 1307-5543 – ejpam.com
Published by New York Business Global

On the Solution of the Fractional-Order Pneumonia Model Using Numerical Computational Methods

Ahmad Alalyani

Department of Mathematics, Faculty of Science, Al-Baha University, Al-Baha, Saudi Arabia

Abstract. This paper deals with the solution and the dynamics of the pneumonia fractional-order mathematical model using numerical computational methods. We study positivity, boundedness, equilibria, local and global stability, and the basic reproductive number $\mathfrak{R}_0$ of the proposed model, which is the one most significant parameter in epidemiological modeling. It estimates the average number of additional infections induced by a sole infectious individual within a fully susceptible group during the mean period of infection. To verify the theoretical analysis of the proposed model, we use numerical techniques including the Adams-Bashforth-Moulton method, the generalized Euler method, the generalized Runge-Kutta method, and the multistep generalized differential transform method. The numerical results and simulations confirm the convergence between the presented fractional-order model and its integer-order form. The proposed model proves to be a valuable tool for investigating dynamical and numerical analysis for a variety of disease models in epidemiology.

2020 Mathematics Subject Classifications: 26A33, 34A08, 34D20, 65L99, 92-10, 92C42, 92D25, 92D30

Key Words and Phrases: Pneumonia disease, Fractional-order mathematical model, Caputo fractional derivative, Stability analysis, Numerical techniques

1. Introduction

According to Johns Hopkins Medicine [34], pneumonia is a disease of one or both of the lungs caused by infection with bacteria, viruses, or fungi. Pneumonia has more than 30 different causes, which are grouped according to the cause. The main species of pneumonia include bacterial pneumonia, viral pneumonia, mycoplasma pneumonia, and other pneumonias. People of different ages can get pneumonia, but the groups at the highest risk are children under the age of 2, adults ages 65 and older, individuals with specific medical conditions, and individuals who smoke. The majority of people with pneumonia have a good reaction to medicine, but pneumonia can be lethal. In 2013, Ong'ala et al. [46] created a mathematical model for pneumonia dynamics with carriers.

DOI: https://doi.org/10.29020/nybg.ejpam.v17i4.5396

Email address: azaher@bu.edu.sa (A. Alalyani)

They use bifurcation and stability of equilibrium points to study the reduction paths or transfer rates between infected individuals and the carriers. In 2014, a simple model of ODE was presented by Mochan et al. [36] to dynamically describe the host's immune response to pneumonia caused by bacteria infection in murine strains. In 2014, Drusano et al. [21] examined how granulates work to kill bacteria and found no role for antibiotics. Ndelwa et al. [39] created in 2015 a mathematical model to describe the pneumonia transmission process in order to estimate transmission and effects. In 2015, Kosasih et al. [29] used wavelet-based crackle detection to analyze a mathematical model of cough sounds for quick identification of pneumonia caused by bacteria in children. Cesar et al. [16] mathematically evaluated in 2016 a fine particulate matter using a model and assessed medicines for pediatric asthma and pneumonia. Atypical bacterial pathogens were recorded as the primary reasons for lower respiratory illnesses such as CAP, bronchitis, and coughs by Marchello et al. [32] in 2016. Cheng et al. in 2017 estimated an IAV-SP model dynamically and mathematically [17]. To develop the respiratory health of COPD patients, they created a quantitative risk-assessment structure. In 2017, Kosasih and Abeyratne [28] proposed a straightforward mathematical model to illustrate the measurement analysis for the clinical identification of pediatric pneumonia.

Tilahun et al. [55] presented in 2017 a non-linear mathematical model along with an analysis of optical control approaches for pneumonia disease. Tilahun et al. [56] considered in 2018 a co-infection model for the diseases of pneumonia and typhoid fever, and their distinctive relation in the case of a treatment and medical plans of action was mathematically analyzed. Based on mathematical characteristics of cough sounds, Raj et al. in 2018 [49] studied the classification of pneumonia and asthma in poor populations. Kizito and Tumwiine [27] provided a mathematical model in 2018 that illustrates how bacteria control the spread of pneumonia. In addition, the dynamics of vaccine formulation and treatment were discussed. A non-linear mathematical model that describes the modeling of co-infection of the influenza A virus and pneumonia within the host was studied in 2018 by Mbabazi et al. [33]. Tilahun in 2019 [54] used theorems and ordinary differential equations to describe a pneumonia-meningitis co-infection model. Tilahun provided an explanation of different disease clearance methods. In 2019, Diah and Aziz [19] reviewed dynamic mathematical models of pneumonia, followed by earlier research. Tilahun in 2019 [53] investigated a mathematical model of co-dynamics for the diseases meningitis and pneumonia. In 2020, Otoo et al. [47] studied a model that illustrates how bacteria spread pneumonia, and the analysis in this study was helpful in determining the effects of vaccination on disease control. In 2020, the graphical result for the dynamics of a mathematical model for pneumonia was provided by Zephaniah et al. [60]. Ming et al. [35] discussed in 2020 the growing number of coronavirus pneumonia cases and the spread of this disease in Wuhan, China. In 2020, Jung et al. [26] exhibited the observations through a variety of clinical tests and revealed a novel pathogen as the cause of disease. In 2021, Wafula et al. [59] established a deterministic mathematical model of pneumonia-HIV co-infection with the utilization of anti-pneumonia and ART therapy strategies as control to describe optimal control treatment. Oluwatobi and Erinle-Ibrahim in 2021 [45] investigated the impact of treating pneumonia disease, the existence of efficient reproduction

numbers, and the stability of equilibrium points. In 2021, a delayed mathematical modeling technique was implemented by Muhammad Naveed et al. [38] to analyze pneumonia disease. Olumuyiwa James Peter et al. in 2021 [44] introduced a model for pneumococcal pneumonia infection using fractional order derivatives in the sense of the Caputo-Fabrizio operator. In 2022, Sayed Saber et al. [52] studied a fractional mathematical SVCIR model to estimate the pneumonia disease transmission dynamics in sheep and goats in Al-Baha region of Saudi Arabia with cost-effective strategies. The research conducted by Sayed Saber et al. investigated critical parameters that impact the transmission of pneumonia in livestock. They provided evidence that the implementation of cost-effective vaccination and treatment strategies led to a substantial reduction in disease prevalence. Furthermore, the fractional models usually have more accurate predictions compared to the traditional integer models. In 2022, Kamaledin Abodayeh et al. [1] discussed the dynamical and numerical analysis of a pneumonia model using appropriate numerical techniques. Fractional epidemic models provide various advantages, such as improved accuracy in representing the memory and hereditary properties of disease transmission. They offer improved capacity to explain the complex dynamics of disease transmission over time, a facet that traditional integer models may neglect. This results in heightened predictive accuracy and more efficacious intervention strategies. There is also substantial literature dealing with the mathematical investigation of a disease model; (see, for example, but not limited to, ([13], [5], [50], [7], [3], [14], [2], [12]).

We develop in this research a fractional-order model for the presented model in [1] to describe the dynamics of transmission for pneumonia disease. More precisely, for any arbitrary time t, a fractional-order SCIR model is taken into consideration in the context of the Caputo derivative $D^{\alpha}, 0 < \alpha \leq 1$, and is provided by:

$$\begin{aligned} D^{\alpha}S(t) &= \Lambda - \frac{\delta(I(t)+\omega C(t))}{N}S(t) - \mu S(t) + \eta R(t), \\ D^{\alpha}C(t) &= \frac{\delta(I(t)+\omega C(t))}{N}\theta S(t) - Z_1 C(t), \\ D^{\alpha}I(t) &= \frac{\delta(I(t)+\omega C(t))}{N}(1-\theta)S(t) + \pi C(t) - Z_2 I(t), \\ D^{\alpha}R(t) &= \beta C(t) + \tau I(t) - (\mu+\eta)R(t), \end{aligned} \tag{1}$$

with the initial conditions $S(0) = S_0$, $C(0) = C_0$, $I(0) = I_0$, and $R(0) = R_0$. Here, the infection force is give by $\frac{\delta(I(t)+\omega C(t))}{N}$. The fractional-order SCIR model, as expressed in Eq. (1), serves as a mathematical representation tailored to elucidate the dynamics of pneumonia transmission. The model employs the Caputo derivative D^{α}, where $0 < \alpha \leq 1$, to incorporate memory effects in the system dynamics. This approach facilitates a more precise characterization of biological processes in the real-world, frequently exhibited by fractional dynamics. Fractional mathematical modeling has been shown to be an effective mathematical tool with uses in a variety of fields of study (see, for example, but not limited to, ([4], [8], [10], [11], [48], [9], [51], [57], [6]). In Eq. (1), $S(t)$ represents the susceptible who is susceptible to infection with pneumonia. $C(t)$ stands for the individuals who carry pneumonia bacteria and can transmit the infection. $I(t)$ stands for the infectious

individuals who have the potential to transfer the infection to the susceptible; and $R(t)$ stands for the individuals who received treatment for pneumonia and made a recovery. Over time, susceptibility to the disease may be regained by these individuals, contingent upon factors such as waning immunity. Λ represents the per capita recruitment rate of new susceptible individuals into the population, which may occur through processes such as births or immigration. δ stands for the transmission rate of pneumonia, denoting the efficiency with which the disease spreads from infectious and carrier individuals to susceptible individuals. ω indicates the rate of treated individuals who had vaccinations. μ stands for the per capita natural death rate of individuals due to non-pneumonia-related causes. η represents the rate of immunity loss in recovered individuals, leading to their return to the susceptible class and accounting for the potential of reinfection. $Z_1 = \mu+\beta+\pi$ is a combined rate representing the sum of (μ), the per capita carriers recovery rate (β), and the rate of developing symptoms by carriers (π). $Z_2 = \tau + \mu + \sigma$ is a combined rate representing the sum of (μ), the per capita recovery rate of infected individuals by pneumonia (τ), and the disease-induced death rate and birth rate of the human population per capita (σ). θ is the rate of susceptible individuals who, following infection, become carriers instead of manifesting symptoms. The total population size, often assumed to be constant, is denoted by N, where $N = S(t) + C(t) + I(t) + R(t)$.

We study the local and global stability of steady states. We derive the fundamental reproduction threshold parameter to show that the disease-free steady state is locally and globally asymptotically stable when $\mathfrak{R}_0 < 1$. However, a positive (endemic) steady state that is both locally and globally asymptotically stable exists when $\mathfrak{R}_0 > 1$. To obtain the approximate solution and verify the theoretical analysis of the fractional-order SCIR model, we have used numerical methods including the Adams-Bashforth-Moulton Method (ABMM), the Generalized Euler Method (GEM), the Generalized Runge-Kutta Method (GRKM), and the Multistep Generalized Differential Transform Method (MSGDTM). The paper is structured as follows: Section 2 discusses the properties of the model. Section 3 investigates the stability analysis of the model. Section 4 explains the numerical computational methods of solution. Sections 5, 6, and 7 present the numerical simulations and results, discussion of the results, and conclusion.

2. Properties of the Model

Let $\mathbb{R}_+$ be the set of all nonnegative real numbers and assume that $\Omega_+ = \{(S, C, I, R) \in \mathbb{R}^4_+ : S \geq 0,\, C \geq 0,\, I \geq 0,\, R \geq 0,\, \max\,(|S|, |C|, |I|, |R|) \leq N\}$.

Theorem 1 ([13]). *If the starting condition $\Gamma_0 = (S(0), C(0), I(0), R(0)) \in \Omega$ is satisfied, then the solution $\Gamma = (S(t), C(t), I(t), R(t)) \in \Omega$ to the model (1) is the only one that can exist for $t \geq 0$.*

Proof. Take

$$\begin{aligned}
\mathfrak{T}_1(\Gamma) &= \Lambda - \frac{\delta I(t)S(t)}{N} - \frac{\delta\omega C(t)S(t)}{N} - \mu S(t) + \delta R(t),\\
\mathfrak{T}_2(\Gamma) &= \frac{\delta\theta I(t)S(t)}{N} + \frac{\delta\omega\theta C(t)S(t)}{N} - Z_1 C(t),\\
\mathfrak{T}_3(\Gamma) &= \frac{\delta(I(t)+\omega C(t))}{N}(1-\theta)S(t) + \pi C(t) - Z_2 I(t),\\
\mathfrak{T}_4(\Gamma) &= \beta C(t) + \tau I(t) - (\mu+\eta)R(t).
\end{aligned}$$

Inputting the values $\Gamma, \overline{\Gamma} \in \Omega$, with $|\frac{\delta(I(t)+\omega C(t))}{N}| \leq K$, yields the following:

$$\begin{aligned}
\|\mathfrak{T}(\overline{\Gamma}) - \mathfrak{T}(\Gamma)\| &= |\mathfrak{T}_1(\overline{\Gamma}) - \mathfrak{T}_1(\Gamma)| + |\mathfrak{T}_2(\overline{\Gamma}) - \mathfrak{T}_2(\Gamma)| + |\mathfrak{T}_3(\overline{\Gamma}) - \mathfrak{T}_3(\Gamma)| + |\mathfrak{T}_4(\overline{X}) - \mathfrak{T}_4(X)|\\
&\leq (3K + \mu - K\theta)|\overline{S} - S| + (Z_1 + \beta + \pi)|\overline{C} - C|\\
&+ (\tau + Z_2)|\overline{I} - I| + (\delta + \mu + \eta)|\overline{R} - R|\\
&\leq \Gamma|\overline{X} - X|,
\end{aligned}$$

where

$$\Gamma = \max\left\{(2\delta(1+\omega) + \beta + Z_1), (2\delta\omega + \pi + \mu), (2\delta + \tau + Z_2), (\delta + \mu + \eta)\right\}.$$

Consequently, the solution to the model (1) exists and is unique iff $H(X)$ satisfies the Lipschitz condition.

Lemma 1 ([31], Lemma 3)**.** Let $u(t)$ be a function meeting the conditions that $D^\alpha u(t)$ exists for every t. Therefore,

$$\begin{cases} D^\alpha u(t) \leq -\lambda u(t) + \mu,\\ u(t_0) = u_{t_0}, \end{cases}$$

where $0 < \alpha < 1$, $(\lambda, \mu) \in \mathbb{R}^2$, $\lambda \neq 0$, and $t_0 \geq 0$ is the initial time. Then,

$$u(t) \leq \Big(u(t_0) - \frac{\mu}{\lambda}\Big)E_{\alpha,1}\Big[-\lambda(t-t_0)^\alpha\Big] + \frac{\mu}{\lambda},$$

where $E_{\alpha,1}(t) = \sum_{k=0}^{\infty} \frac{t^k}{\Gamma(kq+1)} > 0$ is the Mittag Leffler function.

Theorem 2 ([31])**.** *The model (1) has non-negative solutions if and only if $\theta < 1$.*

Proof. We have

$$\begin{aligned}
D^\alpha S(t)|_{S=0} &= \Lambda + \delta R(t) > 0,\\
D^\alpha C(t)|_{C=0} &= \frac{\delta\theta I(t)S(t)}{N} + \frac{\delta\omega\theta C(t)S(t)}{N} > 0,\\
D^\alpha I(t)|_{I=0} &= \frac{\delta\Omega C(t)}{N}(1-\theta)S(t) + \pi C(t) > 0,\\
D^\alpha R(t)|_{R=0} &= \beta C(t) + \tau I(t) > 0.
\end{aligned}$$

Using Lemmas 5 and 6 from [15], we see that the solutions to (1) are non-negative.

Theorem 3 ([13])**.** *Uniformly bounded solutions for the model (1) begin in*

$$\Omega = \left\{ (S, C, I, R) \in \Omega_+ : 0 \leq S + C + I + R \leq \frac{\Lambda}{\mu} \right\}.$$

Proof. Let

$$N(t) = S(t) + C(t) + I(t) + R(t)$$

be the total population at time t. Thus, we have

$$D^\alpha N(t) = \Lambda - \mu N(t) - \sigma I(t) \leq \Lambda - \mu N(t).$$

Thus,

$$D^\alpha N(t) + \mu N(t) \leq \Lambda.$$

It follows from [18] that if M_α is the Mittag-Leffler function, we have

$$0 \leq N(t) \leq N(0) M_\alpha(-\mu t^\alpha) + t^\alpha M_{\alpha,\alpha+1}(-\mu t^\alpha)).$$

Boukhouima et al. [15] yields

$$0 \leq N(t) \leq \frac{\Lambda}{\mu}, \quad t \longrightarrow \infty.$$

For this reason, the solutions of (1) are uniformly limited in the region Ω, beginning with Ω_+.

3. Stability Analysis of the Model

3.1. Equilibria

For $I = C = 0$, we have

$$0 = \Lambda - \mu S(t) + \eta R(t),$$
$$0 = -(\mu + \eta) R(t).$$

Therefore,

$$S_0 = \frac{\Lambda}{\mu}, \quad R_0 = 0.$$

The disease-free equilibrium $E_1 = \left(\frac{\Lambda}{\mu}, 0, 0, 0 \right)$ is easy to obtain.
The pneumonia endemic equilibrium is represented by $E_2 = (S^*, C^*, I^*, R^*)$ for $I^* > 0$, and can be derived by solving the system of equations (1), that is,

$$\begin{cases} D^\alpha S(t) = 0, \\ D^\alpha C(t) = 0, \\ D^\alpha I(t) = 0, \\ D^\alpha R(t) = 0. \end{cases}$$

By taking $\alpha_1 = \dfrac{\theta\pi + (1-\theta)Z_1}{Z_2}$, we have

$$E^* = (S^*, C^*, I^*, R^*),$$

where

$$\begin{aligned}
S^* &= \frac{NZ_1}{\alpha_1+\omega},\\
C^* &= \frac{(\mu+\eta)(\Lambda(\alpha_1+\omega)-\mu NZ_1)}{(\alpha_1+\omega)(\delta Z_1(\mu+\eta)-\eta(\beta+\tau\alpha_1))},\\
I^* &= \frac{\alpha_1(\mu+\eta)(\Lambda(\alpha_1+\omega)-\mu NZ_1)}{(\alpha_1+\omega)(\delta Z_1(\mu+\eta)-\eta(\beta+\tau\alpha_1))},\\
R^* &= \frac{(\beta+\tau\alpha_1)(\Lambda(\alpha_1+\omega)-\mu NZ_1)}{(\alpha_1+\omega)(\delta Z_1(\mu+\eta)-\eta(\beta+\tau\alpha_1))}.
\end{aligned}$$

3.2. The Basic Reproductive Number $\mathfrak{R}_0$

Next-generation matrix theory allows us to deduce that we obtain

$$D^\alpha y = H(y) - \bar{h}(y),$$

if we set $x = (S, R)^{\mathcal{T}}$ and $y = (C, I)^{\mathcal{T}}$, where

$$H(y) = \begin{bmatrix} \frac{\delta\theta I(t)S(t)}{N} + \frac{\delta\omega\theta C(t)S(t)}{N} \\ \frac{\delta(I(t)+\omega C(t))}{N}(1-\theta)S(t) \end{bmatrix}, \quad \bar{h}(y) = \begin{bmatrix} Z_1C(t) \\ -\pi C(t) + Z_2 I(t) \end{bmatrix}.$$

At $E_1 = \left(\dfrac{\Lambda}{\mu}, 0, 0, 0\right)$, the Jacobian matrix of $H(y)$ and $\bar{h}(y)$ w.r.t. C and I may be obtained as follows:

$$H(y) = \begin{bmatrix} H_1 \\ H_2 \end{bmatrix}, \quad \bar{h}(y) = \begin{bmatrix} \bar{h}_1 \\ \bar{h}_2 \end{bmatrix},$$

where

$$\begin{aligned}
H_1 &= \frac{\delta\theta I(t)S(t)}{N} + \frac{\delta\omega\theta C(t)S(t)}{N},\ \bar{h}_1 = Z_1C(t),\\
H_2 &= \frac{\delta(I(t)+\omega C(t))}{N}(1-\theta)S(t),\ \bar{h}_2 = -\pi C(t) + Z_2 I(t).
\end{aligned}$$

Hence, at E_0, the Jacobian matrix of $H(y)$ and $\bar{h}(y)$ is derived by F and Γ, respectively,

$$F = \begin{bmatrix} \frac{\partial H_1}{\partial C} & \frac{\partial H_1}{\partial I} \\ \frac{\partial H_2}{\partial C} & \frac{\partial H_2}{\partial I} \end{bmatrix}, \quad \Gamma = \begin{bmatrix} \frac{\partial \bar{h}_1}{\partial C} & \frac{\partial \bar{h}_1}{\partial I} \\ \frac{\partial \bar{h}_2}{\partial C} & \frac{\partial \bar{h}_2}{\partial I} \end{bmatrix}.$$

Then,

$$\begin{aligned}
\frac{\partial H_1}{\partial C} &= \frac{\delta\omega\theta}{N}S(t), \qquad \frac{\partial H_1}{\partial I} = \frac{\delta\theta}{N}S(t),\\
\frac{\partial H_2}{\partial C} &= \frac{\delta\omega(1-\theta)}{N}S(t), \quad \frac{\partial H_2}{\partial I} = \frac{\delta(1-\theta)}{N}S(t).
\end{aligned}$$

Similarly, we may obtain the Γ entries as:

$$\frac{\partial \bar{h}_1}{\partial C} = Z_1, \quad \frac{\partial \bar{h}_1}{\partial I} = 0,$$
$$\frac{\partial \bar{h}_2}{\partial C} = -\pi, \quad \frac{\partial \bar{h}_2}{\partial I} = Z_2.$$

The entries in A are derived as follows:

$$A = \begin{bmatrix} \frac{\delta\omega\theta S_0}{N} & \frac{\delta\theta S_0}{N} \\ \frac{\delta\omega(1-\theta)S_0}{N} & \frac{\delta(1-\theta)S_0}{N} \end{bmatrix}, \quad B = \begin{bmatrix} Z_1 & 0 \\ -\pi & Z_2 \end{bmatrix}.$$

Thus,

$$B^{-1} = \begin{bmatrix} \frac{1}{Z_1} & \frac{\pi}{Z_1 Z_2} \\ 0 & \frac{1}{Z_2} \end{bmatrix}.$$

Then,

$$A.B^{-1} = \begin{bmatrix} \frac{\delta\omega\theta S_0}{N} & \frac{\delta\theta S_0}{N} \\ \frac{\delta\omega(1-\theta)S_0}{N} & \frac{\delta(1-\theta)S_0}{N} \end{bmatrix} \cdot \begin{bmatrix} \frac{1}{Z_1} & \frac{\pi}{Z_1 Z_2} \\ 0 & \frac{1}{Z_2} \end{bmatrix}.$$

$$A.B^{-1} = \begin{bmatrix} \frac{\Omega\theta\delta S_0}{NZ_1} & \frac{(\pi\omega+Z_1)\theta\delta S_0}{NZ_1Z_2} \\ \frac{\delta\omega(1-\theta)S_0}{NZ_1} & \frac{(\pi\omega+Z_1)\delta(1-\theta)S_0}{NZ_1Z_2} \end{bmatrix}.$$

The eigenvalues of $A.B^{-1}$ can be obtained as:

$$\begin{vmatrix} \lambda - \frac{\Omega\theta\delta S_0}{NZ_1} & \frac{(\pi\omega+Z_1)\theta\delta S_0}{NZ_1Z_2} \\ \frac{\delta\omega(1-\theta)S_0}{NZ_1} & \lambda - \frac{(\pi\omega+Z_1)\delta(1-\theta)S_0}{NZ_1Z_2} \end{vmatrix} = 0.$$

As a result, the eigenvalues are:

$$\lambda_1 = 0,$$
$$\lambda_2 = \frac{(\omega\theta Z_2 + (1-\theta)(\pi\omega + Z_1))\delta S_0}{NZ_1Z_2}.$$

Thus,

$$\mathfrak{R}_0 = \frac{(\omega\theta Z_2 + (1-\theta)(\pi\omega + Z_1))\delta S_0}{NZ_1Z_2}.$$

3.3. Local Stability

The Jacobian matrix of the system (1) along with its elements is presented as:

$$\mathfrak{J}(E_n) = \begin{pmatrix} \mathfrak{J}_{11} & \mathfrak{J}_{12} & \mathfrak{J}_{13} & \mathfrak{J}_{14} \\ \mathfrak{J}_{21} & \mathfrak{J}_{22} & \mathfrak{J}_{23} & \mathfrak{J}_{24} \\ \mathfrak{J}_{31} & \mathfrak{J}_{32} & \mathfrak{J}_{33} & \mathfrak{J}_{34} \\ \mathfrak{J}_{41} & \mathfrak{J}_{42} & \mathfrak{J}_{43} & \mathfrak{J}_{44} \end{pmatrix},$$

where

$$\mathfrak{J}_{11} = -\frac{\delta I(t)}{N} - \frac{\delta\omega C(t)}{N} - \mu,\ \mathfrak{J}_{12} = -\frac{\delta\omega S(t)}{N},\ \mathfrak{J}_{13} = -\frac{\delta S(t)}{N},\ \mathfrak{J}_{14} = \eta,$$
$$\mathfrak{J}_{21} = \frac{\delta\theta I(t)}{N} + \frac{\delta\omega\theta C(t)}{N},\ \mathfrak{J}_{22} = \frac{\delta\omega\theta S(t)}{N} - Z_1,\ \mathfrak{J}_{23} = \frac{\delta\theta S(t)}{N}, \mathfrak{J}_{24} = 0,$$
$$\mathfrak{J}_{31} = \frac{\delta(I(t)+\omega C(t))}{N}(1-\theta),\ \mathfrak{J}_{32} = \frac{\delta\Omega}{N}(1-\theta)S(t) + \pi,$$
$$\mathfrak{J}_{33} = \frac{\delta}{N}(1-\theta)S(t) - Z_2,\ \mathfrak{J}_{34} = 0,$$
$$\mathfrak{J}_{41} = 0,\ \mathfrak{J}_{42} = \beta,\ \mathfrak{J}_{43} = \tau,\ \mathfrak{J}_{44} = -(\mu+\eta).$$

Lemma 2. *The trivial disease equilibrium $E_0 = (0,0,0,0)$ is locally asymptotically stable in Ω.*

Proof. At $E_0 = (0,0,0,0)$, the model (1) has the following Jacobian matrix $J(E_0)$:

$$J(E_0) = \begin{pmatrix} -\mu & 0 & 0 & \eta \\ 0 & -Z_1 & 0 & 0 \\ 0 & \pi & -Z_2 & 0 \\ 0 & \beta & \tau & -(\mu+\eta) \end{pmatrix}.$$

Therefore, we can get the eigenvalues as:

$$J(E_0) = \begin{vmatrix} \lambda+\mu & 0 & 0 & \eta \\ 0 & \lambda+Z_1 & 0 & 0 \\ 0 & \pi & \lambda+Z_2 & 0 \\ 0 & \beta & \tau & \lambda+(\mu+\eta) \end{vmatrix} = 0.$$

Then,

$$(\lambda+\mu)(\lambda+\mu+\eta)\begin{vmatrix} \lambda+Z_1 & 0 \\ \pi & \lambda+Z_2 \end{vmatrix} = 0.$$

Therefore,

$$(\lambda+\mu)(\lambda+\mu+\eta)(\lambda+Z_1)(\lambda+Z_2) = 0. \tag{2}$$

From Equation (2), we have

$$\lambda_1 = -(\lambda+\mu),\ \ \lambda_2 = -(\lambda+\mu+\eta),\ \lambda_3 = -Z_1,\ \ \lambda_4 = -Z_2.$$

Consequently, $\lambda_1, \lambda_2, \lambda_3, \lambda_4$ are all strictly negative roots of Eq. (2). Thus, as determined by the Routh-Hurwitz criterion, it follows that $E_0 = (0,0,0,0)$ is locally asymptotically stable.

Lemma 3. *The disease-free equilibrium $E_1 = \left(\frac{\Lambda}{\mu}, 0, 0, 0\right)$ is locally asymptotically stable in Ω if $\mathfrak{R}_0 < 1$ and is unstable if $\mathfrak{R}_0 > 1$.*

Proof. At $E_1 = \left(\frac{\Lambda}{\mu}, 0, 0, 0\right)$, the model (1) has the following Jacobian matrix $J(E_1)$:

$$J(E_1) = \begin{pmatrix} -\mu & -\frac{\delta\omega S_0}{N} & -\frac{\delta S_0}{N} & \eta \\ 0 & \frac{\delta\omega\theta S_0}{N} - Z_1 & \frac{\delta\theta S_0}{N} & 0 \\ 0 & \frac{\delta\omega(1-\theta)S_0}{N} + \pi & \frac{\delta(1-\theta)S_0}{N} - Z_2 & 0 \\ 0 & \beta & \tau & -(\mu+\eta) \end{pmatrix}.$$

Therefore, we can get the eigenvalues as:

$$J(E_1) = \begin{vmatrix} \lambda+\mu & -\frac{\delta\omega S_0}{N} & -\frac{\delta S_0}{N} & \eta \\ 0 & \lambda - \frac{\delta\omega\theta S_0}{N} + Z_1 & \frac{\delta\theta S_0}{N} & 0 \\ 0 & \frac{\delta\omega(1-\theta)S_0}{N} + \pi & \lambda - \frac{\delta(1-\theta)S_0}{N} + Z_2 & 0 \\ 0 & \beta & \tau & \lambda+(\mu+\eta) \end{vmatrix} = 0.$$

Then,

$$(\lambda+\mu)(\lambda+\mu+\eta) \begin{vmatrix} \lambda - \frac{\delta\omega\theta S_0}{N} + Z_1 & \frac{\delta\theta S_0}{N} \\ \frac{\delta\omega(1-\theta)S_0}{N} + \pi & \lambda - \frac{\delta(1-\theta)S_0}{N} + Z_2 \end{vmatrix} = 0.$$

Therefore,

$$(\lambda+\mu)(\lambda+\mu+\eta) = 0, \tag{3}$$

or

$$\begin{vmatrix} \lambda - \frac{\delta\omega\theta S_0}{N} + Z_1 & \frac{\delta\theta S_0}{N} \\ \frac{\delta\omega(1-\theta)S_0}{N} + \pi & \lambda - \frac{\delta(1-\theta)S_0}{N} + Z_2 \end{vmatrix} = 0.$$

From Eq. (3), we have

$$\lambda_1 = -(\lambda+\mu), \;\; \lambda_2 = -(\lambda+\mu+\eta),$$

or

$$\lambda^2 + c_1\lambda + c_2 = 0,$$

where

$$\begin{aligned} c_1 &= -\frac{\delta\omega\theta S_0}{N} + Z_1 - \frac{\delta(1-\theta)S_0}{N} + Z_2, \\ c_2 &= -\frac{\pi\delta\theta S_0}{N} - \frac{\delta\omega\theta Z_2 S_0}{N} - \frac{\delta(1-\theta)Z_1 S_0}{N} + Z_1 Z_2, \\ c_2 &= -\frac{[\theta\pi + \omega\theta Z_2 + (1-\theta)Z_1]\delta S_0}{N} + Z_1 Z_2, \end{aligned}$$

where

$$Z_1 = \mu + \beta + \pi, \;\; Z_2 = \tau + \mu + \sigma, \;\; S_0 = \frac{\Lambda}{\mu}.$$

As a result, if $c_1 > 0$ and $c_2 > 0$, the Routh-Hurwitz criteria states that E_1 is locally asymptotically stable when $\mathfrak{R}_0 < 1$. When $\mathfrak{R}_0 < 1$ holds, we must demonstrate that $c_1 > 0$ and $c_2 > 0$.

$$\mathfrak{R}_0 = \frac{(\omega\theta Z_2 + (1-\theta)(\pi\omega + Z_1))\delta S_0}{N Z_1 Z_2}.$$

If $\mathfrak{R}_0 < 1$, we have

$$\frac{(\omega\theta Z_2 + Z_1(1-\theta))\delta S_0}{N} < Z_1 Z_2.$$

If $\Gamma = min\{Z_2, Z_1\}$, we have

$$\frac{(\omega\theta + (1-\theta))\delta S_0}{N} < \frac{Z_1 Z_2}{\Gamma}.$$

Thus,

$$\frac{(\omega\theta + (1-\theta))\delta S_0}{N} < Z_1 + Z_2.$$

Then,

$$c_1 = Z_1 + Z_2 - \frac{(\omega\theta + (1-\theta))\delta S_0}{N} > 0.$$

If $\mathfrak{R}_0 < 1$, we have

$$\frac{(\omega\theta Z_2 + (\pi\omega + Z_1)(1-\theta))\delta S_0}{N Z_1 Z_2} < 1,$$

which implies

$$(\omega\theta Z_2 + (\pi\omega + Z_1)(1-\theta))\delta S_0 < N Z_1 Z_2.$$

That is,

$$N Z_1 Z_2 - [\omega\theta Z_2 + (\pi\omega + Z_1)(1-\theta)]\delta S_0 > 0.$$

That is,

$$Z_1 Z_2 - \frac{[\pi\omega(1-\theta) + \omega\theta Z_2 + Z_1(1-\theta)]\delta S_0}{N} > 0,$$

where

$$Z_1 = \mu + \beta + \pi,\ Z_2 = \tau + \mu + \sigma,\ S_0 = \frac{\Lambda}{\mu}.$$

Thus, $c_2 > 0$. For this reason, when $\mathfrak{R}_0 < 1$, E_1 is locally asymptotically stable and unstable when $\mathfrak{R}_0 > 1$.

Lemma 4. *If $\mathfrak{R}_0 > 1$, the pneumonia endemic equilibrium $E_2 = (S^*, C^*, I^*, R^*)$ is locally asymptotically stable in Ω.*

Proof. At $E_2 = (S^*, C^*, I^*, R^*)$, the model (1) has the following Jacobian matrix $J(E_2)$:

$$J(E_2) = \begin{bmatrix} -f_1 - \mu & -f_2 & -f_3 & \eta \\ f_1\theta & f_2\theta - Z_1 & f_3\theta & 0 \\ f_1(1-\theta) & f_2(1-\theta) + \pi & f_3(1-\theta) - Z_2 & 0 \\ 0 & \beta & \tau & -(\mu + \eta) \end{bmatrix},$$

where $f_1 = \dfrac{\delta I^*}{N} + \dfrac{\delta\omega C^*}{N}$, $f_2 = \dfrac{\delta\omega S^*}{N}$, $f_3 = \dfrac{\delta S^*}{N}$, and its characteristic equation is given by:

$$|J(E_2) - \lambda I| = 0.$$

That is,

$$\begin{vmatrix} -f_1-\mu-\lambda & -f_2 & -f_3 & \eta \\ f_1\theta & f_2\theta - Z_1 - \lambda & f_3\theta & 0 \\ f_1(1-\theta) & f_2(1-\theta)+\pi & f_3(1-\theta) - Z_2 - \lambda & 0 \\ 0 & \beta & \tau & -(\mu+\eta)-\lambda \end{vmatrix}$$
$$= \eta \begin{vmatrix} f_1\theta & f_2\theta - Z_1 - \lambda & f_3\theta \\ f_1(1-\theta) & f_2(1-\theta)+\pi & f_3(1-\theta) - Z_2 - \lambda \\ 0 & \beta & \tau \end{vmatrix}$$
$$- (\mu+\eta+\lambda) \begin{vmatrix} -f_1-\mu-\lambda & -f_2 & -f_3 \\ f_1\theta & f_2\theta - Z_1 - \lambda & f_3\theta \\ f_1(1-\theta) & f_2(1-\theta)+\pi & f_3(1-\theta) - Z_2 - \lambda \end{vmatrix} = 0.$$

Thus, the characteristic values are given by:

$$\lambda^4 + \xi_1\lambda^3 + \xi_2\lambda^2 + \xi_3\lambda + \xi_4 = 0,$$

where

$$\begin{aligned}
\xi_1 &= Z_1 + Z_2 - f_2\theta - f_3(1-\theta) + 2\mu + \eta + f_1,\\
\xi_2 &= Z_1Z_2 - f_2Z_2\theta - f_3Z_1(1-\theta) - f_3\pi\theta + (f_1+\mu)(\mu+\eta) + f_1f_2\theta + f_1f_3(1-\theta),\\
\xi_3 &= (2\mu+\eta+f_1)(Z_1Z_2 - f_2Z_2\theta - f_3Z_1(1-\theta) - f_3\pi\theta) + (\mu+f_1)(\mu+\eta)(Z_1+Z_2-f_2\theta)\\
&\quad + (\mu+\eta)f_1f_2\theta + f_1f_2\theta Z_2 + (\mu+\eta)(f_1f_3(1-\theta) + f_1f_3\pi\theta + f_1f_3Z_1(1-\theta)),\\
\xi_4 &= (\mu+f_1)(\mu+\eta)(Z_1Z_2 - f_2Z_2\theta - f_3Z_1(1-\theta) - f_3\pi\theta) + f_1f_2\theta(\mu+\eta)Z_2\\
&\quad + (\mu+\eta)(f_1f_3\pi\theta + f_1f_3Z_1(1-\theta)).
\end{aligned}$$

According to the Routh-Hurwitz criterion for the fourth-degree polynomial, the provided constraint has been verified if $\mathfrak{R}_0 > 1$.

3.4. Global Stability

Theorem 4. *The disease-free equilibrium* $E_1 = \left(\dfrac{\Lambda}{\mu}, 0, 0, 0\right)$ *is globally asymptotically stable in* Ω.

Proof. Take the Lyapunov function with positive definiteness

$$L_2(S, C, I, R) = \left(S - S_0 - S_0 \ln \frac{S}{S_0}\right).$$

From [58], we have

$$D^{\alpha}L_2(S,C,I,R) \leq \Big(\frac{S-S_0}{S}\Big)D^{\alpha}S = \Big(\frac{S-S_0}{S}\Big)\Big(\Lambda - \frac{\delta I(t)S(t)}{N} - \frac{\delta\omega C(t)S(t)}{N} - \mu S(t) + \eta R(t)\Big).$$

At $E_1 = \left(\frac{\Lambda}{\mu}, 0, 0, 0\right)$, we have

$$\begin{aligned}
D^{\alpha}L_2(S,V,C,I,R) &\leq \Big(\frac{S-S_0}{S}\Big)D^{\alpha}S = \Big(\frac{S-S_0}{S}\Big)\Big(\Lambda - \frac{\delta(I(t)+\omega C(t))}{N}S(t) - \mu S(t) + \eta R(t)\Big)\\
&= \Big(S-S_0\Big)\Big(\frac{\Lambda}{S} - \frac{\delta(I(t)+\omega C(t))}{N} - \mu + \frac{\eta R(t)}{S}\Big)\\
&= \Big(S-S_0\Big)\Big(\frac{\Lambda}{S} + \frac{\eta R(t)}{S} - \frac{\Lambda}{S_0} - \frac{\eta R(t)}{S_0}\Big)\\
&= \Big(S-S_0\Big)\Big(-\frac{\Lambda}{SS_0}\Big(S-S_0\Big) - \frac{\eta R(t)}{SS_0}\Big(S-S_0\Big)\Big)\\
&= -\frac{\Lambda}{SS_0}\Big(S-S_0\Big)^2 - \frac{\eta R}{SS_0}\Big(S-S_0\Big)^2.
\end{aligned}$$

Thus, for all $(S,C,I,R) \in \Omega$, $D^{\alpha}L_2(S,C,I,R) < 0$. Therefore, it follows from [30] that E_1 is globally asymptotically stable in Ω.

Theorem 5. *The pneumonia endemic equilibrium $E_2 = (S^*, C^*, I^*, R^*)$ is globally asymptotically stable in Ω.*

Proof. Take the Lyapunov function with positive definiteness

$$\begin{aligned}
L_2(S,C,I,R) = &\Big(S - S^* - S^*\ln\frac{S}{S^*}\Big) + \Big(C - C^* - C^*\ln\frac{C}{C^*}\Big)\\
&+ \Big(I - I^* - I^*\ln\frac{I}{I^*}\Big) + \Big(R - R^* - R^*\ln\frac{R}{R^*}\Big).
\end{aligned}$$

From [58], we have

$$\begin{aligned}
D^{\alpha}L_2(S,V,C,I,R) &\leq \Big(\frac{S-S^*}{S}\Big)D^{\alpha}S + \Big(\frac{C-C^*}{C}\Big)D^{\alpha}C + \Big(\frac{I-I^*}{I}\Big)D^{\alpha}I + \Big(\frac{R-R^*}{R}\Big)D^{\alpha}R\\
&= \Big(\frac{S-S^*}{S}\Big)\Big(\Lambda - \frac{\delta(I+\omega C)}{N}S - \mu S + \eta R\Big)\\
&+ \Big(\frac{C-C^*}{C}\Big)\Big(\frac{\delta(I(t)+\omega C)}{N}\theta S - Z_1 C\Big)\\
&+ \Big(\frac{I-I^*}{I}\Big)\Big(\frac{\delta(I+\omega C)}{N}(1-\theta)S + \pi C - Z_2 I\Big)\\
&+ \Big(\frac{R-R^*}{R}\Big)\Big(\beta C + \tau I - (\mu+\eta)R\Big)
\end{aligned}$$

$$
\begin{aligned}
&= \Big(S - S^*\Big)\Big(\frac{\Lambda}{S} - \frac{\delta(I+\omega C)}{N} - \mu + \frac{\eta R}{S}\Big) \\
&+ \Big(C - C^*\Big)\Big(\frac{\delta(IS)}{NC}\theta + \frac{\delta\omega S}{N}\theta - Z_1\Big) \\
&+ \Big(I - I^*\Big)\Big(\frac{\delta S}{N}(1-\theta) + \frac{\delta\Omega SC}{NI}(1-\theta) + \frac{\pi C}{I} - Z_2\Big) \\
&+ \Big(R - R^*\Big)\Big(\frac{\beta C}{R} + \frac{\tau I(t)}{R} - (\mu+\eta)\Big) \\
&= \Big(S - S^*\Big)\Big(\frac{\Lambda}{NS} + \frac{\eta R}{NS} - \frac{\Lambda}{NS^*} - \frac{\eta R}{NS^*}\Big) \\
&+ \Big(C - C^*\Big)\Big(\frac{\delta(IS)}{NC}\theta - \frac{\delta(IS)}{NC^*}\theta\Big) \\
&+ \Big(I - I^*\Big)\Big(\frac{\delta\Omega SC}{NI}(1-\theta) + \frac{\pi C}{I} - \frac{\delta\Omega SC}{NI^*}(1-\theta) - \frac{\pi C}{I^*}\Big) \\
&+ \Big(R - R^*\Big)\Big(\frac{\beta C}{R} + \frac{\tau I}{R} - \frac{\beta C}{R^*} - \frac{\tau I}{R^*}\Big) \\
&= \Big(S - S^*\Big)\Big(-\frac{\Lambda}{NSS^*}\Big(S - S^*\Big) - \frac{\eta R}{NSS^*}\Big(S - S^*\Big)\Big) \\
&+ \Big(C - C^*\Big)\Big(-\frac{\delta(IS\theta)}{NCC^*}\Big(C - C^*\Big)\Big) \\
&+ \Big(I - I^*\Big)\Big(-\frac{\delta\omega(1-\theta)SC}{NII^*}\Big(I - I^*\Big) - \frac{\pi C}{II^*}\Big(I - I^*\Big)\Big) \\
&+ \Big(R - R^*\Big)\Big(-\frac{\beta C}{NRR^*}\Big(R - R^*\Big) - \frac{\tau I}{NRR^*}\Big(R - R^*\Big)\Big) \\
&= -\frac{\Lambda}{NSS^*}\Big(S - S^*\Big)^2 - \frac{\eta R}{NSS^*}\Big(S - S^*\Big)^2 - \frac{\delta(IS\theta)}{NCC^*}\Big(C - C^*\Big)^2 \\
&- \frac{\delta\omega(1-\theta)SC}{NII^*}\Big(I - I^*\Big)^2 - \frac{\pi C}{II^*}\Big(I - I^*\Big)^2 \\
&- \frac{\beta C}{RR^*}\Big(R - R^*\Big)^2 - \frac{\tau I}{RR^*}\Big(R - R^*\Big)^2.
\end{aligned}
$$

Thus, for all $(S, C, I, R) \in \Omega$, $D^\alpha L_2(S, C, I, R) < 0$. Therefore, it follows from [30] that E_2 is globally asymptotically stable in Ω.

4. Numerical Computational Methods of Solution

In this section, we describe an implementation of the numerical methods we will apply for solving the proposed model (1). The fractional integral $J_m^\alpha f(t)$ of the function $f : \mathbb{R}_+ \longrightarrow \mathbb{R}$ is defined as:

$$J_m^\alpha f(t) = \frac{1}{\Gamma(\alpha)} \int_m^t (t-\theta)^{\alpha-1} f(\theta) d\theta, \quad t \geq m,$$

where $\alpha \in \mathbb{R}_+$ is a non-integer order and $\Gamma(z) = \int_0^\infty e^{-t}t^{z-1}dt$ is the Euler Gamma function.

It follows from [48] that the Caputo fractional derivative $D^\alpha f(t)$ of order $\alpha > 0$, $n-1 < \alpha < n$, $n \in \mathbb{N}$ is defined as:

$$ {}_m^c D^\alpha f(t) = \frac{1}{\Gamma(n-\alpha)} \int_m^t \frac{f^{(n)}(\theta)}{(t-\theta)^{\alpha+1-n}}\, d\theta, \quad t \geq m. $$

4.1. The Adams-Bashforth-Moulton Method (ABMM)

We consider the problem,

$$ \begin{aligned} \mathcal{D}^\alpha\, x(t) &= f(t, x(t)), \quad t \in [0, T], \quad 0 < \alpha \leq 1, \\ x^{(j)}(0) &= x_0^{(j)}, \qquad\quad j = 0, 1, 2, ..., n-1. \end{aligned} \tag{4} $$

Let $h = \dfrac{T}{k}$ be the step size, where k is a positive integer and $T > 0$, and x_j be the approximate solution of $x(t_j)$ at $t = t_j$, where $t_j = jh$, $j = 0, 1, ..., k$.

Take into consideration this integral part,

$$ I_{n+1} = \int_0^{t_{n+1}} (t_{n+1} - \theta)^{\alpha-1} g(\theta)\, d\theta, \quad n = 0, 1, 2, ..., k-1. $$

This can be approximately estimated using the following method

$$ I_{n+1} \approx \int_0^{t_{n+1}} (t_{n+1} - \theta)^{\alpha-1} \widetilde{g}_{n+1}(\theta)\, d\theta, \quad n = 0, 1, 2, ..., k-1, $$

where $\widetilde{g}_{n+1}(\theta)$ is the approximation of $g(\theta)$ on the interval $[0, t_{n+1}]$.

Diethelm et al. [20] carried out the preliminary study on the fractional Adams technique for (1), which may be formulated in the following way:

$$ x_{n+1}^p = \sum_{j=0}^{k-1} \frac{t_{n+1}^j}{j!}\, x_0^{(j)} + \frac{h^\alpha}{\Gamma(\alpha+2)} \sum_{j=0}^{n} \ell_{j,n+1} f(t_j,\, x_j). $$

$$ x_{n+1} = \sum_{j=0}^{k-1} \frac{t_{n+1}^j}{j!} y_0^{(j)} + \frac{h^\alpha}{\Gamma(\alpha+2)} \left(\sum_{j=0}^{n} \ell_{j,n+1} f(t_j,\, x_j) + \ell_{n+1,n+1} f(t_{n+1}, x_{n+1}^p) \right). \tag{5} $$

Here $\ell_{j,n+1}$ are given by

$$ \ell_{j,n+1} = \begin{cases} n^{\alpha+1} - (n-\alpha)(n+1)^\alpha, & \text{if} \quad j = 0, \\ (n-j+2)^{\alpha+1} + (n-j)^{\alpha+1} - 2(n-j+1)^{\alpha+1}, & \text{if} \quad 1 \leq j \leq n, \\ 1, & \text{if} \quad j = n+1. \end{cases} $$

By taking

$$Z_1 = \mu + \beta + \pi, \quad Z_2 = \tau + \mu + \sigma, \tag{6}$$

the model (1) may be reformulated in the sense of the ABMM, according to Eq. (5), as follows:

$$\begin{aligned}
S_{n+1} &= S_0 + \frac{h^\alpha}{\Gamma(\alpha+2)}\Big(\Lambda - \frac{\delta(I^p_{n+1} + \omega C^p_{n+1})}{N} S^p_{n+1} - \mu S^p_{n+1} + \eta R^p_{n+1}\Big) \\
&\quad + \frac{h^\alpha}{\Gamma(\alpha+2)} \sum_{j=0}^{n} \Psi_{j,n+1}\Big(\Lambda - \frac{\delta(I(t_j) + \omega C(t_j))}{N} S(t_j) - \mu S(t_j) + \eta R(t_j)\Big), \\
C_{n+1} &= C_0 + \frac{h^\alpha}{\Gamma(\alpha+2)}\Big(\frac{\delta(I^p_{n+1} + \omega C^p_{n+1})}{N} \theta S^p_{n+1} - Z_1 C^p_{n+1}\Big) \\
&\quad + \frac{h^\alpha}{\Gamma(\alpha+2)} \sum_{j=0}^{n} \Psi_{j,n+1}\Big(\frac{\delta(I(t_j) + \omega C(t_j))}{N} \theta S(t_j) - Z_1 C(t_j)\Big),
\end{aligned}$$

$$\begin{aligned}
I_{n+1} &= I_0 + \frac{h^\alpha}{\Gamma(\alpha+2)}\Big(\frac{\delta(I^p_{n+1} + \omega C^p_{n+1})}{N} (1-\theta) S^p_{n+1} + \pi C^p_{n+1} - Z_2 I^p_{n+1}\Big) \\
&\quad + \frac{h^\alpha}{\Gamma(\alpha+2)} \sum_{j=0}^{n} \Psi_{j,n+1}\Big(\frac{\delta(I(t_j) + \omega C(t_j))}{N} (1-\theta) S(t_j) + \pi C(t_j) - Z_2 I(t_j)\Big), \\
R_{n+1} &= R_0 + \frac{h^\alpha}{\Gamma(\alpha+2)}\Big(\beta C^p_{n+1} + \tau I^p_{n+1} - (\mu+\eta) R^p_{n+1}\Big) \\
&\quad + \frac{h^\alpha}{\Gamma(\alpha+2)} \sum_{j=0}^{n} \Psi_{j,n+1}\Big(\beta C(t_j) + \tau I(t_j) - (\mu+\eta) R(t_j)\Big),
\end{aligned}$$

where $S^p_{n+1}, C^p_{n+1}, I^p_{n+1}$, and R^p_{n+1} are given below:

$$\begin{aligned}
S^p_{n+1} &= S_0 + \frac{h^\alpha}{\Gamma(\alpha+2)} \sum_{j=0}^{n} \Psi_{j,n+1}\Big(\Lambda - \frac{\delta(I(t_j) + \omega C(t_j))}{N} S(t_j) - \mu S(t_j) + \eta R(t_j)\Big), \\
C^p_{n+1} &= C_0 + \frac{h^\alpha}{\Gamma(\alpha+2)} \sum_{j=0}^{n} \Psi_{j,n+1}\Big(\frac{\delta(I(t_j) + \omega C(t_j))}{N} \theta S(t_j) - Z_1 C(t_j)\Big), \\
I^p_{n+1} &= I_0 + \frac{h^\alpha}{\Gamma(\alpha+2)} \sum_{j=0}^{n} \Psi_{j,n+1}\Big(\frac{\delta(I(t_j) + \omega C(t_j))}{N} (1-\theta) S(t_j) + \pi C(t_j) - Z_2 I(t_j)\Big), \\
R^p_{n+1} &= R_0 + \frac{h^\alpha}{\Gamma(\alpha+2)} \sum_{j=0}^{n} \Psi_{j,n+1}\Big(\beta C(t_j) + \tau I(t_j) - (\mu+\eta) R(t_j)\Big).
\end{aligned}$$

4.2. The Generalized Euler Method (GEM)

The extended Euler's method for numerically solving the initial value problem (4) with the Caputo derivatives was derived by Odibat and Momani [43]. First, let's look at the starting value problem. If x, $D^{\alpha}x$, and $D^{2\alpha}x$ are continuous on $[0,b]$ and $a_1,\ldots,a_n$ are positive integer constants, then it follows from (4) that for each value of t, there is a value a_1, which implies

$$x(t)=x(t_0)+(\mathcal{D}^{\alpha}x(t))(t_0)\frac{t^{\alpha}}{\Gamma(\alpha+1)}+(\mathcal{D}^{2\alpha}x(t))(a_1)\frac{t^{2\alpha}}{\Gamma(2\alpha+1)}. \tag{7}$$

Substituting $(\mathcal{D}^{\alpha}x(t))(t_0)=f(t_0,x(t_0))$ and $h=t_1$ into Eq. (7) yields an equation for $x(t_1)$:

$$x(t_1)=x(t_0)+f(t_0,x(t_0))\frac{h^{\alpha}}{\Gamma(\alpha+1)}+(\mathcal{D}^{2\alpha}x(t))(a_1)\frac{h^{2\alpha}}{\Gamma(2\alpha+1)}.$$

If the step size h is sufficiently small, the second-order term (involving $h^{2\alpha}$) may be neglected, allowing us to get

$$x(t_1)=x(t_0)+\frac{h^{\alpha}}{\Gamma(\alpha+1)}f(t_0,x(t_0)).$$

Repeating this procedure yields a sequence of points that estimates the solution $x(t)$. This iterative general formula for the GEM when $t_{j+1}=t_j+h$ is

$$x(t_{j+1})=x(t_j)+\frac{h^{\alpha}}{\Gamma(\alpha+1)}f(t_j,x(t_j)), \tag{8}$$

for $j=0,1,...,k-1$. The model (1) may be reformulated in the sense of GEM, according to Eq. (8), as follows:

$$\begin{aligned}
S(t_{j+1})&=S(t_j)+\frac{h^{\alpha}}{\Gamma(\alpha+1)}\Big(\Lambda-\frac{\delta(I(t_j)+\omega C(t_j))}{N}S(t_j)-\mu S(t_j)+\eta R(t_j)\Big),\\
C(t_{j+1})&=C(t_j)+\frac{h^{\alpha}}{\Gamma(\alpha+1)}\Big(\frac{\delta(I(t_j)+\omega C(t_j))}{N}\theta S(t_j)-Z_1C(t_j)\Big),\\
I(t_{j+1})&=I(t_j)+\frac{h^{\alpha}}{\Gamma(\alpha+1)}\Big(\frac{\delta(I(t_j)+\omega C(t_j))}{N}(1-\theta)S(t_j)+\pi C(t_j)-Z_2I(t_j)\Big),\\
R(t_{j+1})&=R(t_j)+\frac{h^{\alpha}}{\Gamma(\alpha+1)}\Big(\beta C(t_j)+\tau I(t_j)-(\mu+\eta)R(t_j)\Big).
\end{aligned}$$

Through this, we have

$$\begin{aligned}
S_{n+1}&=S_n+\frac{h^{\alpha}}{\Gamma(\alpha+1)}\frac{h^{\alpha}}{\Gamma(\alpha+1)}\Big(\Lambda-\frac{\delta(I_n+\omega C_n)}{N}S_n-\mu S_n+\eta R_n\Big),\\
C_{n+1}&=C_n+\frac{h^{\alpha}}{\Gamma(\alpha+1)}\Big(\frac{\delta(I_n+\omega C_n)}{N}\theta S_n-Z_1C_n\Big),\\
I_{n+1}&=I_n+\frac{h^{\alpha}}{\Gamma(\alpha+1)}\Big(\frac{\delta(I_n+\omega C_n)}{N}(1-\theta)S_n+\pi C_n-Z_2I_n\Big),\\
R_{n+1}&=R_n+\frac{h^{\alpha}}{\Gamma(\alpha+1)}\Big(\beta C_n+\tau I_n-(\mu+\eta)R_n\Big),
\end{aligned}$$

where $0 < \frac{h^\alpha}{\Gamma(\alpha+1)} < 1$ is the step size and subject to the initial conditions, $S(0) = S_0$, $C(0) = C_0$, $I(0) = I_0$, $R(0) = R_0$. We have $S_{n+1} = S_n = S$, $C_{n+1} = C_n = C$, $I_{n+1} = I_n = I$, and $R_{n+1} = R_n = R$ at a fixed point.

4.3. The Generalized Runge-Kutta Method (GRKM)

The numerical scheme of Equation (4) of the GRKM takes the following form:

$$\begin{aligned} x_{n+1} &= x_n + \frac{1}{6}\Big(K_1 + 2K_2 + 2K_3 + K_4\Big), \\ K_1 &= \hbar f(t_n, x_n), \\ K_2 &= \hbar f(t_n + \frac{1}{2}\hbar, x_n + \frac{1}{2}K_1), \\ K_3 &= \hbar f(t_n + \frac{1}{2}\hbar, x_n + \frac{1}{2}K_2), \\ K_4 &= \hbar f(t_n + \hbar, x_n + K_3), \end{aligned} \tag{9}$$

where $\bar{h} = \dfrac{h^\alpha}{\Gamma(\alpha+1)}$.

In the sense of (9), the numerical scheme of (1) of the GRKM takes the following form:

$$\begin{aligned} S_{n+1} &= S_n + \frac{1}{6}\Big(K_1 + 2K_2 + 2K_3 + K_4\Big), \\ C_{n+1} &= C_n + \frac{1}{6}\Big(Q_1 + 2Q_2 + 2Q_3 + Q_4\Big), \\ I_{n+1} &= I_n + \frac{1}{6}\Big(O_1 + 2O_2 + 2O_3 + O_4\Big), \\ R_{n+1} &= R_n + \frac{1}{6}\Big(P_1 + 2P_2 + 2P_3 + P_4\Big), \end{aligned}$$

where $K_1, Q_1, O_1, P_1, K_2, Q_2, O_2, P_2, K_3, Q_3, O_3, P_3, K_4, Q_4, O_4$, and P_4 are given below:

$$\begin{aligned} K_1 &= \bar{h} f_1(t_n, S_n, C_n, I_n, R_n) = \bar{h}\Big(\Lambda - \frac{\delta(I_n + \omega C_n)}{N} S_n - \mu S_n + \eta R_n\Big), \\ Q_1 &= \bar{h} f_2(t_n, S_n, C_n, I_n, R_n) = \bar{h}\Big(\frac{\delta(I_n + \omega C_n)}{N}\theta S_n - Z_1 C_n\Big), \\ O_1 &= \bar{h} f_3(t_n, S_n, C_n, I_n, R_n) = \bar{h}\Big(\frac{\delta(I_n + \omega C_n)}{N}(1-\theta) S_n + \pi C_n - Z_2 I_n\Big), \\ P_1 &= \bar{h} f_4(t_n, S_n, C_n, I_n, R_n) = \bar{h}\Big(\beta C_n + \tau I_n - (\mu + \eta) R_n\Big), \\ K_2 &= \bar{h} f_1\Big(t_n + \frac{1}{2}\bar{h}, S_n + \frac{1}{2}K_1, C_n + \frac{1}{2}Q_1, I_n + \frac{1}{2}O_1, R_n + \frac{1}{2}P_1\Big), \\ Q_2 &= \bar{h} f_2\Big(t_n + \frac{1}{2}\bar{h}, S_n + \frac{1}{2}K_1, C_n + \frac{1}{2}Q_1, I_n + \frac{1}{2}O_1, R_n + \frac{1}{2}P_1\Big), \\ O_2 &= \bar{h} f_3\Big(t_n + \frac{1}{2}\bar{h}, S_n + \frac{1}{2}K_1, C_n + \frac{1}{2}Q_1, I_n + \frac{1}{2}O_1, R_n + \frac{1}{2}P_1\Big), \\ P_2 &= \bar{h} f_4\Big(t_n + \frac{1}{2}\bar{h}, S_n + \frac{1}{2}K_1, C_n + \frac{1}{2}Q_1, I_n + \frac{1}{2}O_1, R_n + \frac{1}{2}P_1\Big), \end{aligned}$$

$$K_3 = \bar{h} f_1\Big(t_n + \frac{1}{2}\bar{h}, S_n + \frac{1}{2}K_2, C_n + \frac{1}{2}Q_2, I_n + \frac{1}{2}O_2, R_n + \frac{1}{2}P_2\Big),$$
$$Q_3 = \bar{h} f_2\Big(t_n + \frac{1}{2}\bar{h}, S_n + \frac{1}{2}K_2, C_n + \frac{1}{2}Q_2, I_n + \frac{1}{2}O_2, R_n + \frac{1}{2}P_2\Big),$$
$$O_3 = \bar{h} f_3\Big(t_n + \frac{1}{2}\bar{h}, S_n + \frac{1}{2}K_2, C_n + \frac{1}{2}Q_2, I_n + \frac{1}{2}O_2, R_n + \frac{1}{2}P_2\Big),$$
$$P_3 = \bar{h} f_4\Big(t_n + \frac{1}{2}\bar{h}, S_n + \frac{1}{2}K_2, C_n + \frac{1}{2}Q_2, I_n + \frac{1}{2}O_2, R_n + \frac{1}{2}P_2\Big),$$
$$K_4 = \bar{h} f_1(t_n + \bar{h}, S_n + K_3, C_n + Q_3, I_n + O_3, R_n + P_3),$$
$$Q_4 = \bar{h} f_2(t_n + \bar{h}, S_n + K_3, C_n + Q_3, I_n + O_3, R_n + P_3),$$
$$O_4 = \bar{h} f_3(t_n + \bar{h}, S_n + K_3, C_n + Q_3, I_n + O_3, R_n + P_3),$$
$$P_4 = \bar{h} f_4(t_n + \bar{h}, S_n + K_3, C_n + Q_3, I_n + O_3, R_n + P_3).$$

4.4. The Multistep Generalized Differential Transform Method (MSGDTM)

To illustrate the MSGDTM following ([42], [24], [22], [25]), we consider the following initial value problem for systems of fractional differential equations:

$$\begin{aligned} \mathcal{D}_1^{\alpha} x_1(t) &= f_1(t, x_1, x_2, ..., x_n), \\ \mathcal{D}_2^{\alpha} x_1(t) &= f_2(t, x_1, x_2, ..., x_n), \\ &\vdots \\ \mathcal{D}_n^{\alpha} x_1(t) &= f_n(t, x_1, x_2, ..., x_n), \end{aligned} \tag{10}$$

subject to the initial conditions:

$$x_i(t_0) = c_i, \qquad i = 1, 2, ..., n, \tag{11}$$

where $\mathcal{D}^{\alpha}$ is the Caputo fractional derivative of order α_i, $i = 1, 2, ..., n$. The initial value problem solution (10), (11) is looked in the range $[t_0, T]$. In real-world applications of the extended differential transform technique, the finite series defines the k^{th} order approximation solution of (4)

$$x_i(t) = \sum_{i=0}^{K} \mathfrak{L}_i(k)(t - t_0)^{k\alpha_i}, \quad t \in [t_0, T],$$

where $\mathfrak{L}_i(k)$ satisfied the (recurrence relation):

$$\frac{\Gamma((k+1)\alpha_i + 1)}{\Gamma(k\alpha_i + 1)} \mathfrak{L}_i(k+1) = F_i(k, \mathfrak{L}_1, \mathfrak{L}_2, ..., \mathfrak{L}_n),$$

$\mathfrak{L}_i(0) = c_i$, and $F_i(k, \mathfrak{L}_1, \mathfrak{L}_2, ..., \mathfrak{L}_n)$ is the differential transform of function fit, $f_i(t, x_1, x_2, ..., x_n)$ for $i = 1, 2, ..., n$. The basic steps of the GDTM can be found in ([41], [37], [40], [23]).

Assume that $[t_0, T]$ is partitioned into M subintervals $[t_{m-1}, t_m]$, $m = 1, 2, ..., M$, with steps $h = \dfrac{T - t_0}{M}$ using the nodes $t_m = t_0 + mh$. The MSGDTM principles are listed below.

First, the GDTM solves (10), (11) throughout the interval $[t_0, t_1]$. We get the approximate solution by beginning with $x_{i,1}(t)$, $t \in [t_0, t_1]$, for $i = 1, 2, ..., n$. For $m \geq 2$, applying the GDTM to (10), (11) across the interval $[t_{m-1}, t_m]$ will employ the IC $x_{i,m}(t_{m-1}) = x_{i,m-1}(t_{m-1})$. Repeating the technique yields approximations for $x_{i,m}(t)$, $m = 1, 2, ..., M$, for $i = 1, 2, ..., n$. The MSGDTM concludes:

$$x_i(t) = \begin{cases} x_{i,1}(t), & \text{for } t \in [t_0, t_1], \\ x_{i,2}(t), & \text{for } t \in [t_1, t_2], \\ \vdots & \\ x_{i,M}(t), & \text{for } t \in [t_{M-1}, t_M]. \end{cases}$$

The MSGDTM is efficient for all values of h. The new algorithm's key benefit is that the solution converges over vast time periods, as we shall show in the following section.

Regarding (1), the MSGDTM algorithm produces

$$\begin{aligned}
\mathbb{S}(k+1) &= \frac{\Gamma(q_1 k + 1)}{\Gamma(q_1(k+1) + 1)} \Big(\Lambda - \frac{\delta(\mathbb{I}(k) + \omega \mathbb{C}(k))}{N} \mathbb{S}(k) - \mu \mathbb{S}(k) + \eta \mathbb{R}(k) \Big), \\
\mathbb{C}(k+1) &= \frac{\Gamma(q_2 k + 1)}{\Gamma(q_2(k+1) + 1)} \Big(\frac{\delta(\mathbb{I}(k) + \omega \mathbb{C}(k))}{N} \theta \mathbb{S}(k) - Z_1 \mathbb{C}(k) \Big), \\
\mathbb{I}(k+1) &= \frac{\Gamma(q_3 k + 1)}{\Gamma(q_3(k+1) + 1)} \Big(\frac{\delta(\mathbb{I}(k) + \omega \mathbb{C}(k))}{N} (1 - \theta) \mathbb{S}(k) + \pi \mathbb{C}(k) - Z_2 \mathbb{I}(k) \Big), \\
\mathbb{R}(k+1) &= \frac{\Gamma(q_4 k + 1)}{\Gamma(q_4(k+1) + 1)} \Big(\beta \mathbb{C}(k) + \tau \mathbb{I}(k) - (\mu + \eta) \mathbb{R}(k) \Big),
\end{aligned}$$

where $\mathbb{S}(k)$, $\mathbb{C}(k)$, $\mathbb{I}(k)$, and $\mathbb{R}(k)$ are the differential transformations of $S(k)$, $C(k)$, $I(k)$, and $R(k)$, respectively. The differential transform of the starting conditions is provided by the formulas $\mathbb{S}(0) = c_1$, $\mathbb{C}(0) = c_2$, $\mathbb{I}(0) = c_3$, and $\mathbb{R}(0) = c_4$, respectively. Through the differential inverse transform, we may find the differential transform series solution for the problem (1):

$$\begin{aligned}
S(t) &= \sum_{n=0}^{K} \mathbb{S}(n) t^{q_1 n}, \\
C(t) &= \sum_{n=0}^{K} \mathbb{C}(n) t^{q_2 n}, \\
I(t) &= \sum_{n=0}^{K} \mathbb{I}(n) t^{q_3 n}, \\
R(t) &= \sum_{n=0}^{K} \mathbb{R}(n) t^{q_4 n}.
\end{aligned}$$

For the MSGDTM, the proposed series solution of (1) is:

$$S(t)=\begin{cases}\sum_{n=0}^{K}\mathbb{S}_1(n)t^{q_1n}, & \text{for } t\in[0,t_1]\\ \sum_{n=0}^{K}\mathbb{S}_2(n)(t-t_1)^{q_1n}, & \text{for } t\in[t_1,t_2]\\ \vdots & \\ \sum_{n=0}^{K}\mathbb{S}_M(n)(t-t_{M-1})^{q_1n}, & \text{for } t\in[t_{M-1},t_M]\end{cases} \tag{12}$$

$$C(t)=\begin{cases}\sum_{n=0}^{K}\mathbb{C}_1(n)t^{q_2n}, & \text{for } t\in[0,t_1]\\ \sum_{n=0}^{K}\mathbb{C}_2(n)(t-t_1)^{q_2n}, & \text{for } t\in[t_1,t_2]\\ \vdots & \\ \sum_{n=0}^{K}\mathbb{C}_M(n)(t-t_{M-1})^{q_2n}, & \text{for } t\in[t_{M-1},t_M]\end{cases} \tag{13}$$

$$I(t)=\begin{cases}\sum_{n=0}^{K}\mathbb{I}_1(n)t^{q_3n}, & \text{for } t\in[0,t_1]\\ \sum_{n=0}^{K}\mathbb{I}_2(n)(t-t_1)^{q_3n}, & \text{for } t\in[t_1,t_2]\\ \vdots & \\ \sum_{n=0}^{K}\mathbb{I}_M(n)(t-t_{M-1})^{q_3n}, & \text{for } t\in[t_{M-1},t_M]\end{cases} \tag{14}$$

$$R(t)=\begin{cases}\sum_{n=0}^{K}\mathbb{R}_1(n)t^{q_4n}, & \text{for } t\in[0,t_1]\\ \sum_{n=0}^{K}\mathbb{R}_2(n)(t-t_1)^{q_4n}, & \text{for } t\in[t_1,t_2]\\ \vdots & \\ \sum_{n=0}^{K}\mathbb{R}_M(n)(t-t_{M-1})^{q_4n}, & \text{for } t\in[t_{M-1},t_M],\end{cases} \tag{15}$$

where $\mathbb{S}_i(n)$, $\mathbb{C}_i(n)$, $\mathbb{I}_i(n)$, and $\mathbb{R}_i(n)$ for $i=1,2,...,M$ satisfy the following (recurrence relations):

$$\begin{aligned}
\mathbb{S}_i(k+1)&=\frac{\Gamma(q_1k+1)}{\Gamma(q_1(k+1)+1)}\Big(\Lambda-\frac{\delta(\mathbb{I}_i(k)+\omega\mathbb{C}_i(k))}{N}\mathbb{S}_i(k)-\mu\mathbb{S}_i(k)+\eta\mathbb{R}_i(k)\Big),\\
\mathbb{C}_i(k+1)&=\frac{\Gamma(q_2k+1)}{\Gamma(q_2(k+1)+1)}\Big(\frac{\delta(\mathbb{I}_i(k)+\omega\mathbb{C}_i(k))}{N}\theta\mathbb{S}_i(k)-Z_1\mathbb{C}_i(k)\Big),\\
\mathbb{I}_i(k+1)&=\frac{\Gamma(q_3k+1)}{\Gamma(q_3(k+1)+1)}\Big(\frac{\delta(\mathbb{I}_i(k)+\omega\mathbb{C}_i(k))}{N}(1-\theta)\mathbb{S}_i(k)+\pi\mathbb{C}_i(k)-Z_2\mathbb{I}_i(k)\Big),\\
\mathbb{R}_i(k+1)&=\frac{\Gamma(q_4k+1)}{\Gamma(q_4(k+1)+1)}\Big(\beta\mathbb{C}_i(k)+\tau\mathbb{I}_i(k)-(\mu+\eta)\mathbb{R}_i(k)\Big),
\end{aligned} \tag{16}$$

with $\mathbb{S}_i(0)=S_i(t_{i-1})=S_{i-1}(t_{i-1})$, $\mathbb{C}_i(0)=C_i(t_{i-1})=C_{i-1}(t_{i-1})$, $\mathbb{I}_i(0)=I_i(t_{i-1})=I_{i-1}(t_{i-1})$, and $\mathbb{R}_i(0)=R_i(t_{i-1})=R_{i-1}(t_{i-1})$. Finally, we start with $\mathbb{S}_0(0)=c_1$, $\mathbb{C}_0(0)=c_2$, $\mathbb{I}_0(0)=c_3$, and $\mathbb{R}_0(0)=c_4$, using the (recurrence relations) (16), then we can get the multistep solution (12)-(15).

5. Numerical Simulations and Results

Using the mathematical software programs: MATLAB and Mathematica and the parameter values listed in Table 1, which are taken from [1], we present numerical simulations and results in this section.

Table 1: The Parameter Values

Parameter	Value / Source [1]
Λ	0.5
δ	2 (DFE) 2.5 (EE)
ω	0.1124
μ	0.5
η	0.00641
β	0.515
π	0.7096
θ	0.563
τ	0.641
σ	0.53

5.1. Numerical Simulations and Results of the ABMM Method

In this subsection, we present numerical simulations and results for the model (1) solution applying the ABMM method.

The solution to the proposed model (1) using the Adams-Bashforth-Moulton Method appears in Figures 1(a, b, c, d) and Figures 2(a, b, c, d, e). According to these figures, we observe that $S(t)$ increases at $\alpha = 1$ than in the case where α is a fractional variant. We also note that $C(t)$, $I(t)$, and $R(t)$ decrease at $\alpha = 1$ than in the case where α is a fractional variant.

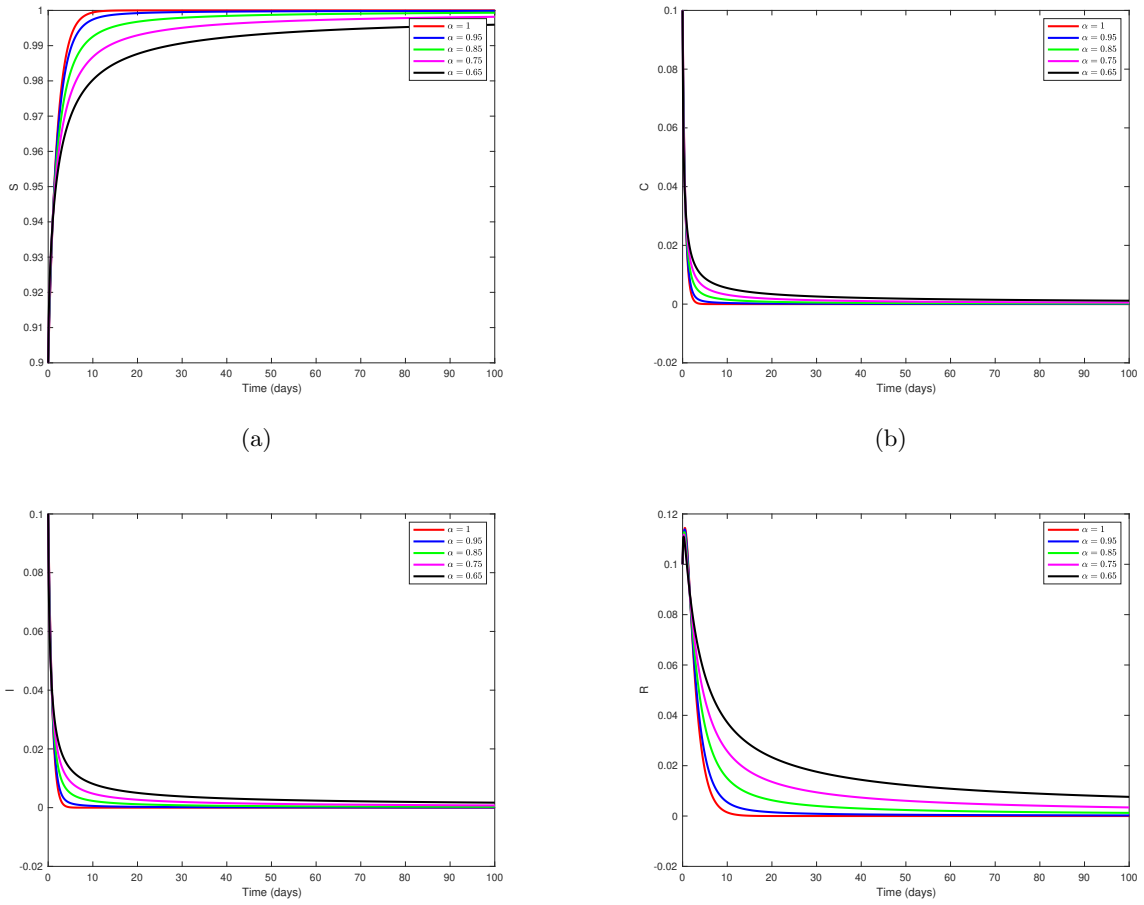

Figure 1: The ABMM method for the behavior of $S(t)$, $C(t)$, $I(t)$, and $R(t)$ at various values of $\alpha = 0.65, 0.75, 0.85, 0.95, 1$.

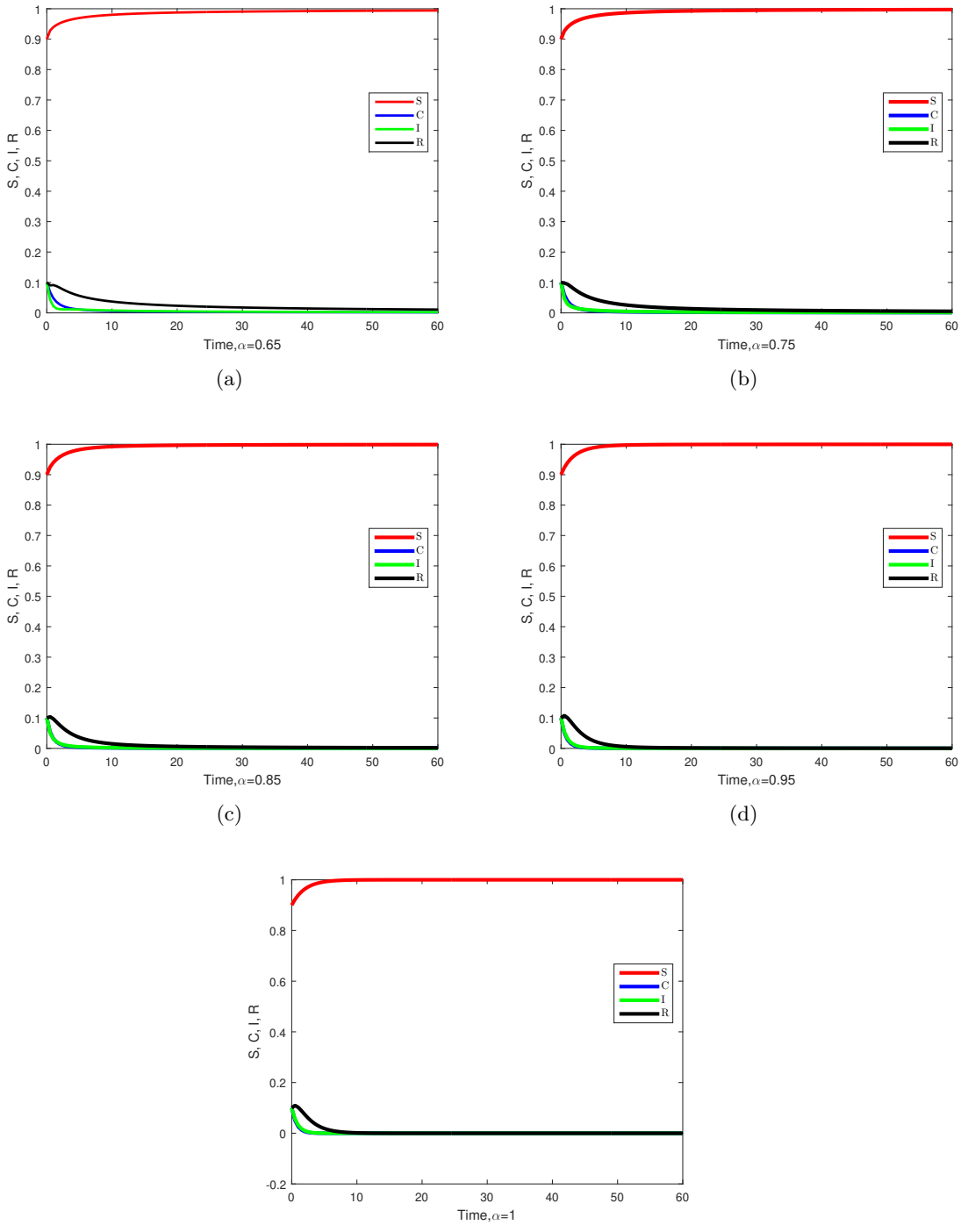

Figure 2: Combined graphical behaviors of the ABMM method for $S(t)$, $C(t)$, $I(t)$, and $R(t)$ at various values of $\alpha = 0.65, 0.75, 0.85, 0.95, 1$.

5.2. Numerical Simulations and Results of the GEM Method

In this subsection, we present numerical simulations and results for the model (1) solution applying the GEM method.

The solution to the proposed model (1) using the Generalized Euler Method appears in Figures 3(a, b, c, d) and Figures 4(a, b, c, d, e). According to these figures, we observe that $S(t)$ increases at $\alpha = 1$ than in the case where α is a fractional variant. We also note that $C(t)$ and $I(t)$ decrease at $\alpha = 1$ than in the case where α is a fractional variant. For $R(t)$, the dynamical behavior increases at $\alpha = 1$ in the first days and then gets remarkably decreased, as well as in the case where α is a fractional variant.

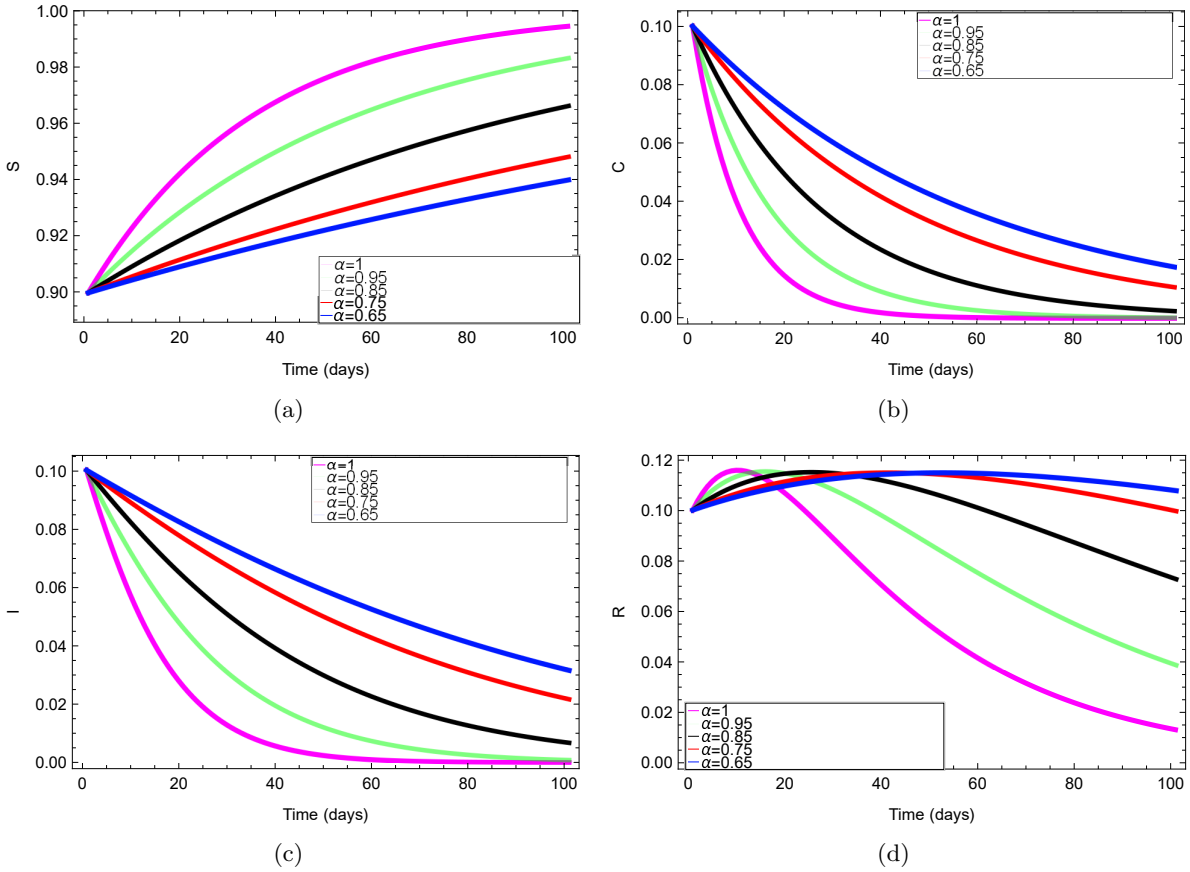

Figure 3: The GEM method for the behavior of $S(t)$, $C(t)$, $I(t)$, and $R(t)$ at various values of $\alpha = 0.65, 0.75, 0.85, 0.95, 1$.

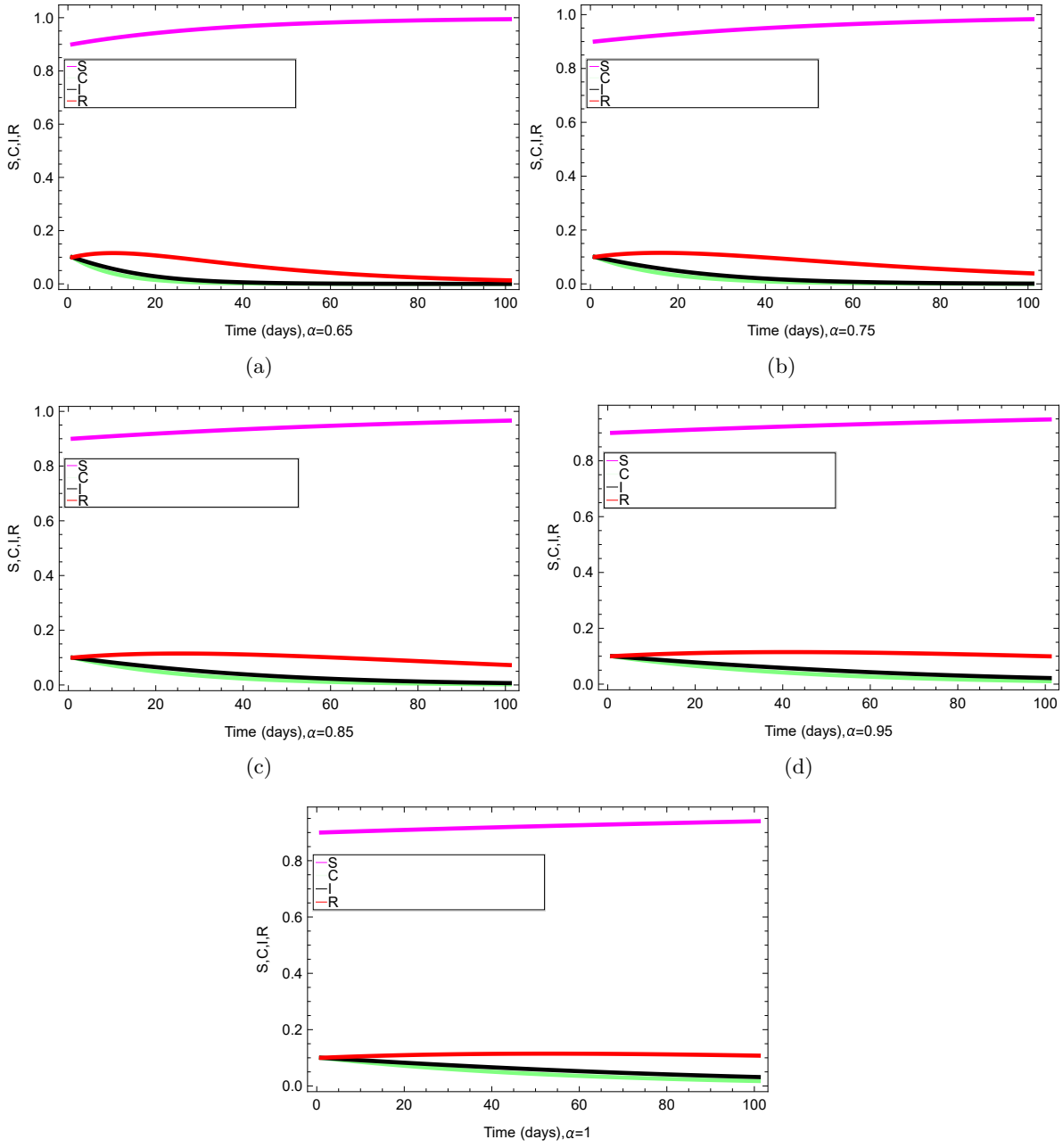

Figure 4: Combined graphical behaviors of the GEM method for $S(t)$, $C(t)$, $I(t)$, and $R(t)$ at various values of $\alpha = 0.65, 0.75, 0.85, 0.95, 1$.

5.3. Numerical Simulations and Results of the GRKM Method

In this subsection, we present numerical simulations and results for the model (1) solution applying the GRKM method.

In Figures 5(a, b, c, d) and Figures 6(a, b, c, d, e), we present the solution to the proposed model (1) using the Generalized Runge-Kutta Method. According to these figures, we observe that $S(t)$ increases more in the case where α is a fractional variant than in the case where $\alpha = 1$. We also note that $C(t)$, $I(t)$, and $R(t)$ decrease more in the case where α is a fractional variant than in the case where $\alpha = 1$.

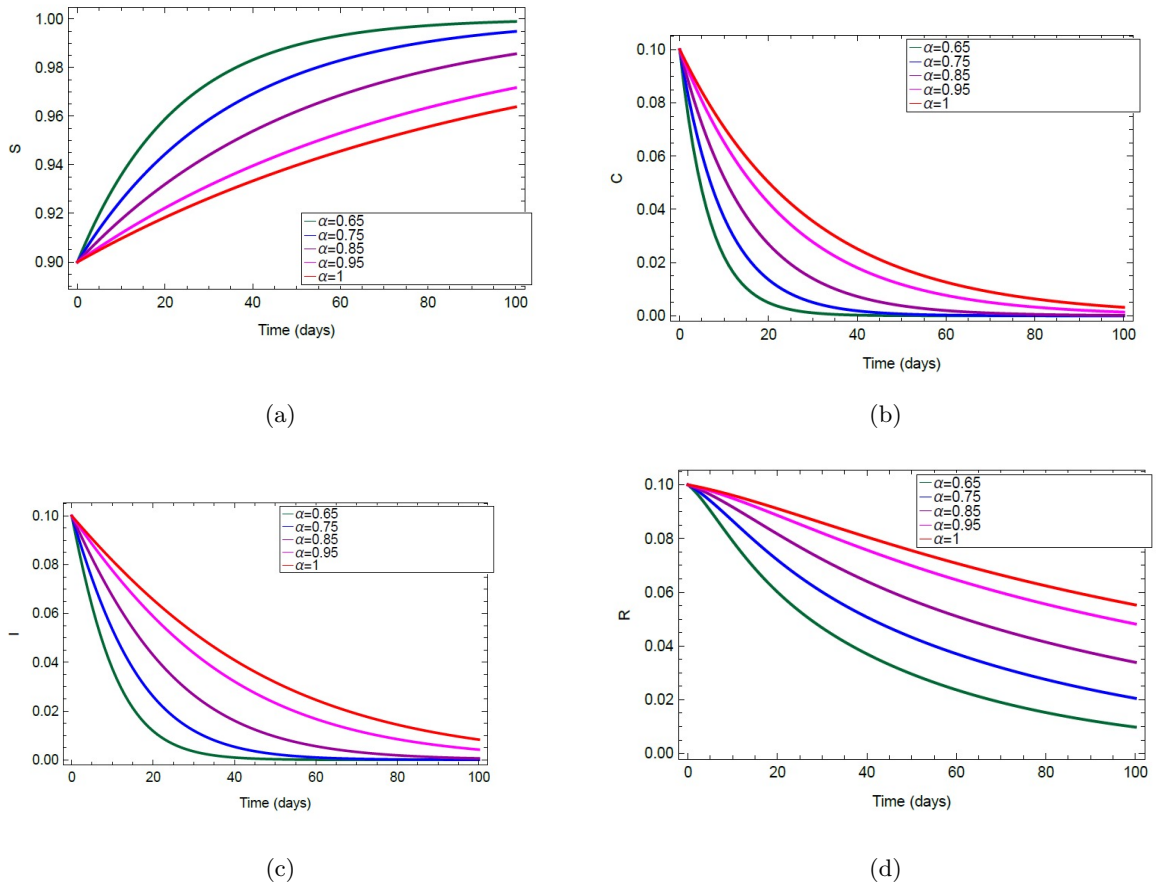

Figure 5: The GRKM method for the behavior of $S(t)$, $C(t)$, $I(t)$, and $R(t)$ at various values of $\alpha = 0.65, 0.75, 0.85, 0.95, 1$.

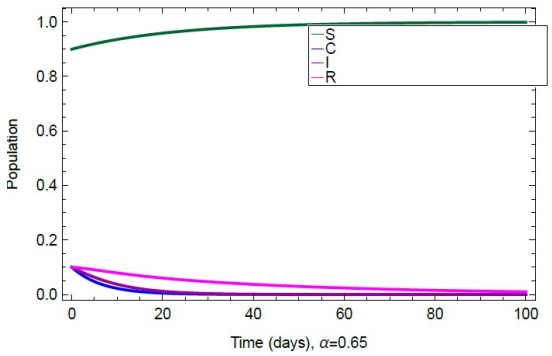

(a)

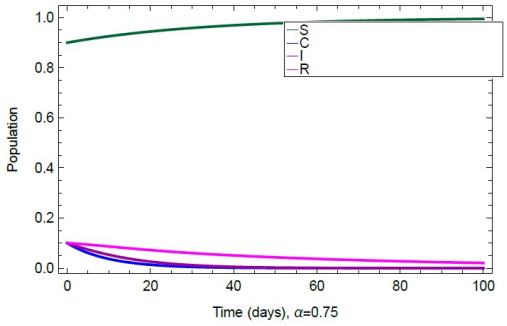

(b)

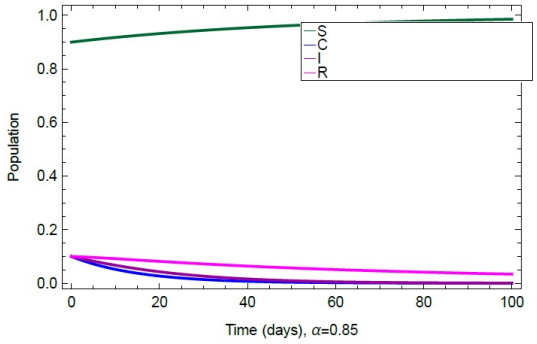

(c)

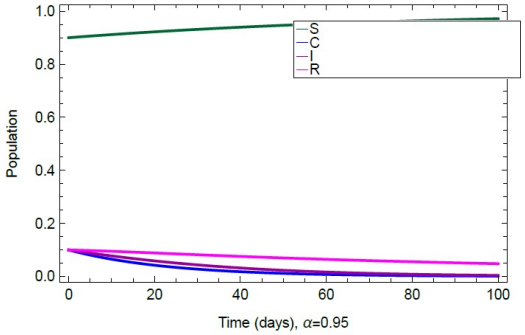

(d)

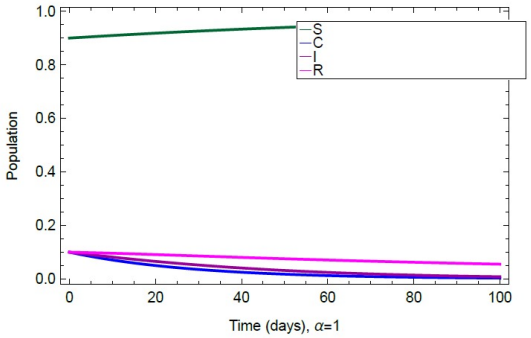

(e)

Figure 6: Combined graphical behaviors of the GRKM method for $S(t)$, $C(t)$, $I(t)$, and $R(t)$ at various values of $\alpha = 0.65, 0.75, 0.85, 0.95, 1$.

5.4. Numerical Simulations and Results of the MSGDTM Method

In this subsection, we present numerical simulations and results for the model (1) solution applying the MSGDTM method.

The solution to the proposed model (1) using the Multistep Generalized Differential Transform Method appears in Figures 7(a, b, c, d) and Figures 8(a, b, c, d, e). According to these figures, we observe that $S(t)$ remarkably increases in the case where α is a fractional variant than in the case where $\alpha = 1$. We also note that $C(t)$, $I(t)$, and $R(t)$ remarkably decrease in a similar way for both cases where α is a fractional variant and $\alpha = 1$.

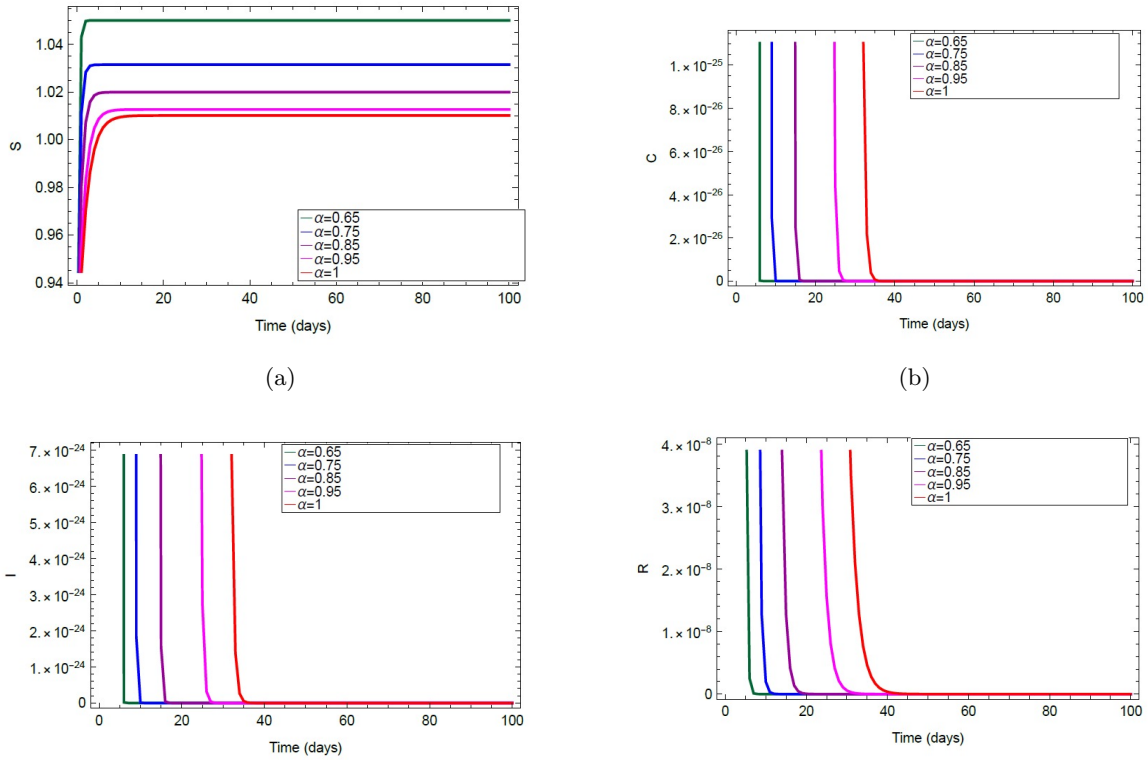

Figure 7: The MSGDTM method for the behavior of $S(t)$, $C(t)$, $I(t)$, and $R(t)$ at various values of $\alpha = 0.65, 0.75, 0.85, 0.95, 1$.

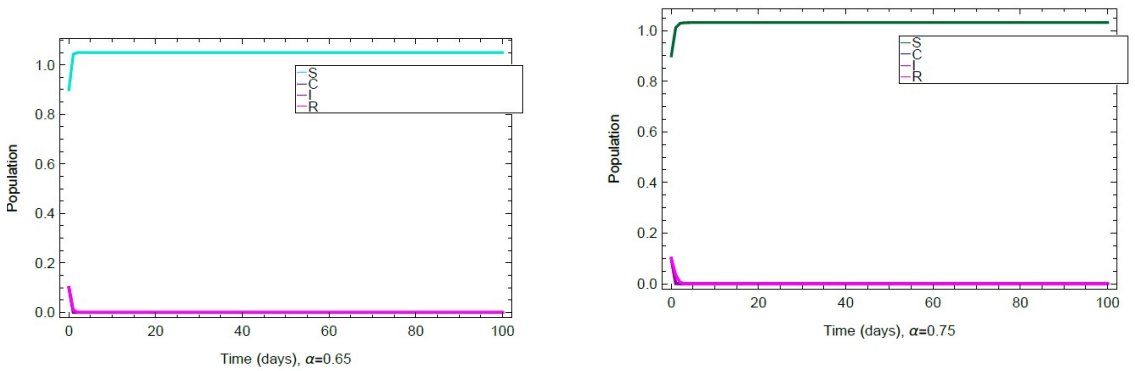

(a)

(b)

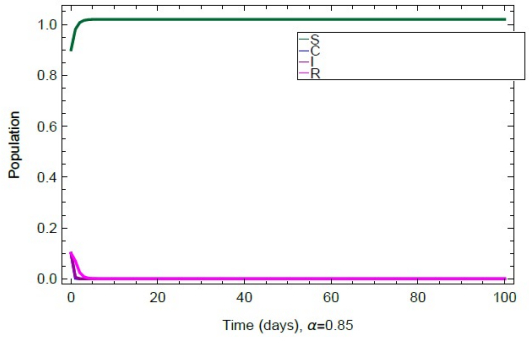

(c)

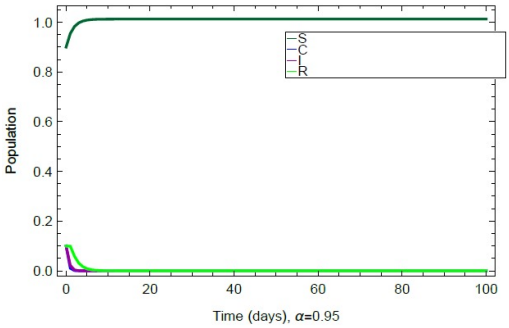

(d)

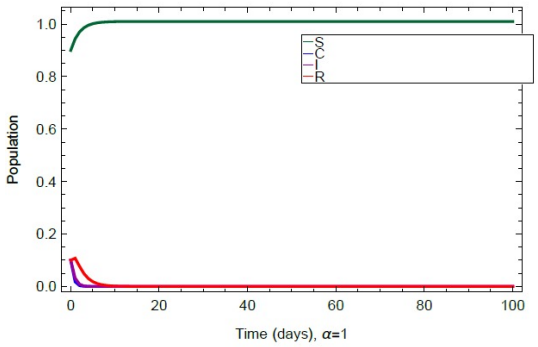

(e)

Figure 8: Combined graphical behaviors of the MSGDTM method for $S(t)$, $C(t)$, $I(t)$, and $R(t)$ at various values of $\alpha = 0.65, 0.75, 0.85, 0.95, 1$.

6. Discussion of the Results

We present the solution to the proposed model (1) using four different numerical methods. From the numerical simulations and results in Section 5, we observe that the solution to the proposed model (1) gets stable faster using the ABMM and the MSGDTM methods than using the GEM and the GRKM methods. The solution to the proposed model (1) using the ABMM method gets stable faster in the case where $\alpha = 1$ than in the case where α is a fractional variant. On the other hand, the solution to the proposed model (1) using the MSGDTM method gets stable faster in the case where α is a fractional variant than in the case where $\alpha = 1$. From numerical simulations and results, we can say that the numerical methods we used are efficient computational methods. The ABMM, the GEM, the GRKM, and the MSGDTM exhibit greater flexibility and applicability across a diverse spectrum of problems, with a specific emphasis on initial value problems and systems of ordinary differential equations (ODEs). The improved shooting method, specialized for boundary value problems (BVPs), exhibits high accuracy, stability, and robustness when applied to coupled nonlinear higher-order systems. It is generally the preferred method for dealing with BVPs, particularly in complex nonlinear intricate.

7. Conclusion

In this work, we investigated the solution and the dynamics of the pneumonia fractional-order mathematical model (1) using numerical techniques including the Adams-Bashforth-Moulton method, the generalized Euler method, the generalized Runge-Kutta method, and the multistep generalized differential transform method. For the sake of the analysis of the proposed model (1), we discussed positivity, boundedness, equilibria, local and global stability, and the basic reproductive number $\mathfrak{R}_0$. Based on the numerical simulations, we observed that there is a convergence in results between the proposed fractional-order mathematical model (1) and its integer-order form. The aim of using the fractional-order mathematical model (1) is to investigate the memory of the model for a long time period; that is, at any time t, the fractional-order mathematical model investigates the behavior of the variables $S(t)$, $C(t)$, $I(t)$, and $R(t)$ during the period $[0, 1]$ as a result of changing the values of α, while the integer-order form investigates the behavior of the variables only at $\alpha = 1$. This was useful in investigating the stability of the model during the period $[0, 1]$ as a result of changing the values of α and gaining a better understanding of the disease's dynamics. This work will also be a valuable tool for different types of disease modeling. The figures presented in this paper illustrate the dynamic behavior of the system variables $S(t)$, $C(t)$, $I(t)$, and $R(t)$ under various fractional orders α using four different numerical methods: the Adams-Bashforth-Moulton Method (ABMM), the Generalized Euler Method (GEM), the Generalized Runge-Kutta Method (GRKM), and the Multistep Generalized Differential Transform Method (MSGDTM).

The main contribution of these figures lies in conducting a comparative analysis of the four different methods used to approximate solutions for the proposed fractional-order mathematical model. Specifically, Figures 1 and 2, obtained using the ABMM method,

and Figures 3 and 4, obtained employing the GEM method, illustrate that $S(t)$ exhibits an increase, while $C(t)$, $I(t)$, and $R(t)$ all decrease as the fractional order α approaches 1. This observation indicates that the behavior of integer-order dynamics diverges notably from that of fractional-order dynamics, and the depicted figures highlight the model's sensitivity to fractional variations. Figures 5 and 6, obtained using the GRKM method, illustrate a reverse trend where $S(t)$ increases more for fractional values of α compared to $\alpha = 1$, while $C(t)$, $I(t)$, and $R(t)$ decrease, emphasizing the impact of employing a fractional order in the model. Figures 7 and 8, obtained using the MSGDTM method, demonstrate a remarkable increase in $S(t)$ for fractional values of α compared to $\alpha = 1$, while $C(t)$, $I(t)$, and $R(t)$ consistently decrease, reinforcing the consistent behavior observed across various methods. The collective results indicate that fractional-order models offer a more nuanced and accurate representation of system dynamics when compared to integer-order models. Additionally, the selection of a numerical method significantly impacts the accuracy and stability of the solutions. The visual comparisons presented in the figures play a pivotal role in comprehending distinctions and in choosing suitable numerical techniques for fractional-order differential equations.

Acknowledgements

The author expresses gratitude to the editor and referees for their time and insightful comments.

References

[1] K. Abodayeh, A. Raza, M. Rafiq, M. Shoaib Arif, M. Naveed, et al. Analysis of Pneumonia Model via Efficient Computing Techniques. *Computers, Materials & Continua*, 70(3):6073–6088, 2022.

[2] Khalid Ahmed, Haroon Adam, M.Y. Youssif, and Sayed Saber. Different strategies for diabetes by mathematical modeling: Applications of fractal-fractional derivatives in the sense of atangana-baleanu. *Results in Physics*, 52:106892, 2023.

[3] Khalid Ahmed, Haroon Adam, M.Y. Youssif, and Sayed Saber. Different strategies for diabetes by mathematical modeling: Modified minimal model. *Alex. Eng. J.*, 80:74–87, 2023.

[4] Khalid I.A. Ahmed, Haroon D.S. Adam, Najat Almutairi, and Sayed Saber. Analytical solutions for a class of variable-order fractional liu system under time-dependent variable coefficients. *Results in Physics*, 56:107311, 2024.

[5] S. Al-Zahrani, Fathelrhman Guma, K. Al-Zahrani, and Sayed Saber. A Fractional Order SITR Model for Forecasting of Transmission of COVID-19: Sensitivity Statistical Analysis. *Malaysian Journal of Mathematical Sciences*, 16(3):517–536, 2022.

[6] Ahmad Alalyani. On the Solution of a Nonlinear Fractional-Order Glucose-Insulin System Incorporating β-cells Compartment. *Malaysian Journal of Mathematical Sciences*, 17(1):1–12, 2023.

[7] Ahmad Alalyani and Sayed Saber. Stability analysis and numerical simulations of the fractional COVID-19 pandemic model. *Int. J. Nonlin. Sci. Num.*, 24(3):989–1002, 2023.

[8] N. Almutairi and S. Saber. On chaos control of nonlinear fractional newton-leipnik system via fractional caputo-fabrizio derivatives. *Scientific Reports*, 13:22726, 2023.

[9] Najat Almutairi and Sayed Saber. Chaos control and numerical solution of time-varying fractional Newton-Leipnik system using fractional Atangana-Baleanu derivatives. *AIMS Mathematics*, 8(11):25863–25887, 2023.

[10] Najat Almutairi and Sayed Saber. Application of a time-fractal fractional derivative with a power-law kernel to the burke-shaw system based on newton's interpolation polynomials. *MethodsX*, 12:102510, 2024.

[11] Najat Almutairi and Sayed Saber. Existence of chaos and the approximate solution of the Lorenz–Lü–Chen system with the Caputo fractional operator. *AIP Advances*, 14(1):015112, 2024.

[12] Najat Almutairi, Sayed Saber, and Hijaz Ahmad. The fractal-fractional Atangana-Baleanu operator for pneumonia disease: stability, statistical and numerical analyses. *AIMS Mathematics*, 8(12):29382–29410, 2023.

[13] M. H. Alshehri, F. Z. Duraihem, A. Alalyani, and S. Saber. A Caputo (discretization) fractional-order model of glucose-insulin interaction: Numerical solution and comparisons with experimental data. *J. Taibah Univ. Sci.*, 15(1):26–36, 2021.

[14] Mansoor H. Alshehri, Sayed Saber, and Faisal Z. Duraihem. Dynamical analysis of fractional-order of ivgtt glucose–insulin interaction. *Int. J. Nonlin. Sci. Num.*, 24:1123–1140, 2023.

[15] A. Boukhouima, K. Hattaf, and N. Yousfi. Dynamics of a fractional order hiv infection model with specific functional response and cure rate. *Int. J. Differ. Equ.*, 2017:Article ID 8372140, 2017.

[16] A.C.G. Cesar, L.F.C. Nascimento, K.C.C. Mantovani, and L.C.P. Vieira. Fine particulate matter estimated by mathematical model and hospitalisations for pneumonia and asthma in children. *Rev. Paul. Pediatr. (Engl. Ed.)*, 34(1):18–23, 2016.

[17] Y.H. Cheng, S.H. You, Y.J. Lin, S.C. Chen, W.Y. Chen, W.C. Chou, and C.M. Liao. Mathematical modeling of post coinfection with influenza a virus and streptococcus pneumoniae, with implications for pneumonia and copd-risk assessment. *Int. J. Chronic Obstr. Pulm. Dis.*, 12:1973–1988, 2017.

[18] S.K. Choi, B. Kang, and N. Koo. Stability for caputo fractional differential systems. *Abstr. Appl. Anal.*, 2014:Article ID 631419, 2014.

[19] I.M. Diah and N. Aziz. Stochastic modelling for pneumonia incidence: a conceptual framework. *AIP Conference Proceedings New York*, 1:1–3, 2019.

[20] K. Diethelm and A. D. Freed. The fracpece subroutine for the numerical solution of differential equations of fractional order. *Forschung und wissenschaftliches Rechnen*, 1999:57–71, 2002.

[21] G.L. Drusano, W. Liu, S. Fikes, R. Cirz, N. Robbins, S. Kurhanewicz, and A. Louie. Interaction of drug-and granulocyte-mediated killing of pseudomonas aeruginosa in a murine pneumonia model. *J. Infect. Dis.*, 210(8):1319–1324, 2014.

[22] V. Erturk, G. Zaman, and S. Momani. A numeric-analytic method for approximating a giving up smoking model containing fractional derivatives. *Computers & Mathematics with Applications*, 64(10):3065–3074, 2012.

[23] V. S. Erturk, S. Momani, and Z. Odibat. Application of generalized differential transform method to multi-order fractional differential equations. *Communications in Nonlinear Science and Numerical Simulation*, 13(8):1642–1654, 2008.

[24] V. S. Erturk, Z. M. Odibat, and S. Momani. An approximate solution of a fractional order differential equation model of human T-cell lymphotropic virus I (HTLV-I) infection of CD4 T-cells. *Computers & Mathematics with Applications*, 62(3):996–1002, 2011.

[25] Asad Freihat and Shaher Momani. Application of multistep generalized differential transform method for the solutions of the fractional-order chua's system. *Discrete Dynamics in Nature and Society*, 2012:Article ID 427393, 2012.

[26] S.M. Jung, R. Kinoshita, R.N. Thompson, N.M. Linton, Y. Yang, A.R. Akhmetzhanov, and H. Nishiura. Epidemiological identification of a novel pathogen in real-time: analysis of the atypical pneumonia outbreak in Wuhan, China, 2019-2020. *J. Clin. Med.*, 9(3):1–18, 2020.

[27] M. Kizito and J. Tumwiine. A mathematical model of treatment and vaccination interventions of pneumococcal pneumonia infection dynamics. *J. Appl. Math.*, 2018:Article ID 2539465, 2018.

[28] K. Kosasih and U. Abeyratne. Exhaustive mathematical analysis of simple clinical measurements for childhood pneumonia diagnosis. *World J. Pediatr.*, 13(5):446–456, 2017.

[29] K. Kosasih, U.R. Abeyratne, V. Swarnkar, and R. Triasih. Wavelet augmented cough analysis for rapid childhood pneumonia diagnosis. *IEEE Trans. Biomed. Eng.*, 62(4):1185–1194, 2015.

[30] J.P. LaSalle. *The Stability of Dynamical Systems.* SIAM, Philadelphia, 1976.

[31] H.L. Li, L. Zhang, C. Hu, et al. Dynamical analysis of a fractional-order predator-prey model incorporating a prey refuge. *J. Appl. Math. Comput.*, 54(1-2):435–449, 2017.

[32] C. Marchello, A.P. Dale, T.N. Thai, D.S. Han, and M.H. Ebell. Prevalence of atypical pathogens in patients with cough and community-acquired pneumonia: a meta-analysis. *Ann. Fam. Med.*, 14(6):552–566, 2016.

[33] F.K. Mbabazi, J.Y.T. Mugisha, and M. Kimathi. Modeling the within-host coinfection of influenza a virus and pneumococcus. *Appl. Math. Comput.*, 339:488–506, 2018.

[34] Johns Hopkins Medicine. Johns hopkins medicine: Pneumonia. Report n.d., Johns Hopkins Medicine, n.d.

[35] W.K. Ming, J. Huang, and C.J. Zhang. Breaking down of healthcare system: mathematical modelling for controlling the novel coronavirus (2019-ncov) outbreak in wuhan, china. *BioRxiv*, 1:1–18, 2020.

[36] E. Mochan, D. Swigon, G. Ermentrout, S. Luken, and G.A. Clermont. Mathematical model of intrahost pneumococcal pneumonia infection dynamics in murine strains. *J. Theor. Biol.*, 353:44–54, 2014.

[37] S. Momani and Z. Odibat. A novel method for nonlinear fractional partial differential equations: combination of DTM and generalized Taylor's formula. *Journal of Computational and Applied Mathematics*, 220(1-2):85–95, 2008.

[38] M. Naveed, D. Baleanu, A. Raza, et al. Modeling the transmission dynamics of delayed pneumonia-like diseases with a sensitivity of parameters. *Adv. Differ. Equ.*, 2021:468, 2021.

[39] E.J. Ndelwa, M. Kgosimore, E.S. Massawe, and L. Namkinga. Mathematical modelling and analysis of treatment and screening of pneumonia. *Math. Theory Model.*, 5(10):21–39, 2015.

[40] Z. Odibat and S. Momani. A generalized differential transform method for linear partial differential equations of fractional order. *Applied Mathematics Letters*, 21(2):194–199, 2008.

[41] Z. Odibat, S. Momani, and V. S. Erturk. Generalized differential transform method: application to differential equations of fractional order. *Applied Mathematics and Computation*, 197(2):467–477, 2008.

[42] Z. M. Odibat, C. Bertelle, M. A. Aziz-Alaoui, and G. H. E. Duchamp. A multistep differential transform method and application to non-chaotic or chaotic systems. *Computers & Mathematics with Applications*, 59(4):1462–1472, 2010.

[43] Z.M. Odibat and S. Momani. An algorithm for the numerical solution of differential equations of fractional order. *J. Appl. Math. Inform.*, 26(1-2):15–27, 2008.

[44] J.P. Olumuyiwa, A. Yusuf, K. Oshinubi, F.A. Oguntolu, J.O. Lawal, A.I. Abioye, and T.A. Ayoola. Fractional order of pneumococcal pneumonia infection model with caputo fabrizio operator. *Results in Physics*, 29:104–581, 2021.

[45] K.I. Oluwatobi and L.M. Erinle-Ibrahim. Mathematical modeling of pneumonia dynamics of children under the age of five. *Res. Square*, 1:1–16, 2021.

[46] J. Ong'ala, P. Oleche, and J.Y.T. Mugisha. Mathematical model for pneumonia dynamics with carriers. *Int. J. Math. Anal.*, 7(50):2457–2473, 2013.

[47] D. Otoo, P. Opoku, S. Charles, and A.P. Kingsley. Deterministic epidemic model for (svcsycasyir) pneumonia dynamics, with vaccination and temporal immunity. *Infect. Dis. Model.*, 5:42–60, 2020.

[48] I. Podlubny. *Fractional Differential Equations.* Academic Press, New York, NY, USA, 1999.

[49] M. Raj, M. Reddy, M. Mufeed, and S. Karthika. HMM based cough sound analysis for classifying asthma and pneumonia in paediatric population. *Int. J. Pure Appl. Math.*, 118(18):609–616, 2018.

[50] S. Saber and A. Alalyani. Stability analysis and numerical simulations of ivgtt glucose-insulin interaction models with two time delays. *Math. Model. Anal.*, 27:383–407, 2022.

[51] Sayed Saber. Control of Chaos in the Burke-Shaw system of fractal-fractional order in the sense of Caputo-Fabrizio. *Journal of Applied Mathematics and Computational Mechanics*, 23(1):83–96, 2024.

[52] Sayed Saber, Azza M. Alghamdi, Ghada A. Ahmed, and Khulud M. Alshehri. Mathematical modelling and optimal control of pneumonia disease in sheep and goats in Al-Baha region with cost-effective strategies. *AIMS Mathematics*, 7(7):12011–12049, 2022.

[53] G.T. Tilahun. Modeling co-dynamics of pneumonia and meningitis diseases. *Adv. Differ. Equ.*, 2019(1):1, 2019.

[54] G.T. Tilahun. Optimal control analysis of pneumonia and meningitis coinfection. *Comput. Math. Methods Med.*, 2019:1–15, 2019.

[55] G.T. Tilahun, O.D. Makinde, and D. Malonza. Modelling and optimal control of pneumonia disease with cost-effective strategies. *J. Biol. Dyn.*, 11(2):400–426, 2017.

[56] G.T. Tilahun, O.D. Makinde, and D. Malonza. Co-dynamics of pneumonia and typhoid fever diseases with cost-effective optimal control analysis. *Appl. Math. Comput.*, 316:438–459, 2018.

[57] R. Ullah, R. Ellahi, S. M. Sait, and S. T. Mohyud-Din. On the fractional order model of HIV-1 infection of $CD4^+$ T-cells under the influence of antiviral drug treatment. *J. Taibah. Univ. Sci.*, 14(1):50–59, 2020.

[58] C. Vargas-De-León. Volterra-type lyapunov functions for fractional-order epidemic systems. *Commun. Nonlinear Sci. Numer. Simul.*, 24:75–85, 2015.

[59] N.M. Wafula, B.O. Kwach, and V.N. Marani. Mathematical modeling and optimal control for controlling pneumonia- HIV coinfection. *Int. J. Innov. Res. Dev.*, 10(1):138–144, 2021.

[60] O.C. Zephaniah, U.I.R. Nwaugonma, I.S. Chioma, and O. Adrew. A mathematical model and analysis of an SVEIR model for streptococcus pneumonia with saturated incidence force of infection. *Math. Model. Appl.*, 5(1):16, 2020.